Received: 27 June 2017 | Revised: 29 March 2018 | Accepted: 24 May 2018 | Published on: 9 August 2018

DOI: 10.1002/joc.5731

International Journal of Climatology RMetS

RESEARCH ARTICLE

The impact of Arctic sea ice on the inter-annual variations of summer Ural blocking

Ruonan Zhang[1,2] | Chenghu Sun[3,4] | Renhe Zhang[1] | Liwei Jia[5] | Weijing Li[4,6]

[1]Department of Atmospheric and Oceanic Sciences & Institute of Atmospheric Sciences, Fudan University, Shanghai, China

[2]Shanghai Institute of Pollution Control and Ecological Security, Shanghai, China

[3]National Meteorological Information Center, China Meteorological Administration, Beijing, China

[4]Collaborative Innovation Center on Forecast and Evaluation of Meteorological Disasters, Nanjing University of Information Science & Technology, Nanjing, China

[5]NOAA Climate Prediction Center/Innovim LLC, College Park, Maryland

[6]National Climate Center, China Meteorological Administration, Beijing, China

Correspondence
Chenghu Sun, National Meteorological Information Center, China Meteorological Administration, No. 46, Zhongguancun Nandajie, Beijing 100081, China.
Email: sunch@cma.gov.cn

Funding information
National Natural Science Foundation of China, Grant/Award Numbers: 41505053417309594179047 2, 41505053, 41730959, 41790472; China Special Fund for Meteorological Research in the Public Interest, Grant/Award Number: GYHY201406018; National Basic Research Program of China, Grant/Award Number: 2013CB430203

The influence of Arctic sea ice concentration (SIC) on the inter-annual variations of the frequency of summertime Ural blocking (UB) during the period of 1980–2013 is investigated using observational and reanalysis data sets and version 5.0 of the Community Atmospheric Model. The results reveal that the variations in the UB frequency display a statistically significant association with a persistent spring–summer SIC pattern in the Barents Sea. Related to high UB frequencies, heavy SICs exert a dynamic influence by increasing the meridional temperature gradient (MTG) in the lower troposphere and cause stronger (weaker) zonal winds in high-latitude (mid-latitude) areas through the thermal wind balance. This zonal wind pattern establishes the background conditions for the blocking activity and thus helps to initiate summertime UB events. Moreover, persistent heavy SICs tend to enhance the low-level atmospheric baroclinicity to the south and decreases in mid-latitude areas, inducing weakened synoptic-scale transient eddy activity (STEA) that stretches from eastern Europe to the Ural Mountains. This reduced STEA is accompanied by a locally intensified eddy-vorticity forcing that may exert a downstream influence on the onset of UB events. In terms of thermodynamic processes, heavy SICs-induced water vapour content anomalies are expected to cause deficits in precipitation over the East European Plateau in late spring and subsequently desiccate the underlying soil. Both of these effects are expected to increase surface heat fluxes and thickness of the lower-middle troposphere, thus favouring anomalous anticyclonic circulation over the Ural Mountains. On the other hand, the opposite dynamic and thermodynamic effects are expected to result from light SICs with respect to low UB frequencies. Therefore, these two effects identified in this study each contribute to an increased probability of more frequent (rare) UB events in summer as the spring–summer sea ice within the regions surrounding the Barents Sea expands (disappears).

KEYWORDS

Arctic sea ice, inter-annual variations, numerical simulations, soil moisture, Ural blocking frequency

1 | INTRODUCTION

Summer droughts and floods over southern China are strongly affected by atmospheric blocking over the Ural Mountains, which favours the equatorwards penetration of cold air masses from high-latitude regions. When these cold air masses encounter moist, warm air masses from the tropical ocean, heavy flooding frequently occurs in southern

China; thus, these processes strongly affect a significant part of the population of China (Tao, 1980; Zhang and Tao, 1998; 2001; Wang and Gu, 2016). Therefore, it is essential to better understand the inter-annual variations in Ural blocking (UB) activity during the summer and the associated mechanisms that produce changes in this blocking.

Over the past several decades, the overall Arctic sea ice extent and concentration undergone rapid declines, particularly in summer and autumn; these declines are argued to represent the effects of Arctic amplification and have a strong influence on the occurrence of extreme climate events in winter, such as cold spells and blocking events in mid-latitude regions (Tang *et al*., 2014; Simmonds, 2015). Moreover, the inter-annual variability in Arctic sea ice has also been found to play an important role in driving extreme weather events in mid-latitude regions (Honda *et al*., 2009; Luo *et al*., 2016a). Therefore, this study examines the impacts of Arctic sea ice on UB activity.

The wintertime responses of atmospheric circulation to changes in Arctic sea ice in autumn and winter have been extensively examined in both observational and modelling analysis (Petoukhov and Semenov, 2010; Li and Wang, 2012; Liu *et al*., 2012; Tang *et al*., 2013; Luo *et al*., 2016a; 2016b). A variety of circulation changes have been identified, such as the occurrence of the warm Arctic–cold Eurasia pattern (Liu *et al*., 2012; Tang *et al*., 2013; Mori *et al*., 2014; Luo *et al*., 2016a), the negative phase of the winter North Atlantic Oscillation (Jaiser *et al*., 2012; Liu *et al*., 2012; Luo *et al*., 2016b), and mid-latitude teleconnections (Dethloff *et al*., 2006; Wu *et al*., 2009a; 2013; Liu *et al*., 2014). In addition, changes in the Arctic may also exert an influence on UB through propagation of the North Atlantic–Eurasian wave train (Wu *et al*., 1999; 2011; Dethloff *et al*., 2006; Liu and Alexander, 2007; Liu *et al*., 2014; Sato *et al*., 2014; Simmonds and Govekar, 2014; Wang and Chen, 2014; Woollings *et al*., 2014; Sun *et al*., 2016a) and the eddy-driven mid-latitude jet stream anomaly over the North Atlantic (Deser *et al*., 2007; Cheung and Zhou, 2015). For example, Murray and Simmonds (1995) and Tang *et al*. (2013) suggested that losses of Arctic sea ice would lead to a decrease in the surface meridional temperature gradient (MTG) between the mid-latitude and polar regions and weakened upper-level zonal winds, which they interpreted as favouring the persistence of extreme events. Recently, Yao *et al*. (2017) further noted that the mid-latitude mean westerly would weaken, increasing the quasi-stationarity and persistence of UB under Arctic warming. However, Screen *et al*. (2013a; 2013b), Mori *et al*. (2014), and Sun *et al*. (2016b) have argued that the remote responses in winter are relatively small relative to the internal variability, whereas the responses in summer are reasonably large (Petrie *et al*., 2015).

Compared with the research findings mentioned above that address the winter season, the impact of Arctic sea ice declines on mid-latitude circulation patterns in summer has received less attention and is thus not well understood. A few studies, such as Wu *et al*. (2013), have suggested that the retreat of sea ice from winter to the following spring in the western Greenland Sea may represent a potential precursor of anomalous summer circulation over northern Eurasia associated with a high-pressure ridge around the Ural Mountains. Using numerical experiments, Petrie *et al*. (2015) found that the anomalous response of the summer Euro-Atlantic wave train to the large decline in Arctic sea ice since 2007 has been dominated by an anticyclonic anomaly over Greenland and a cyclonic anomaly over northwestern Europe. Tang *et al*. (2014) implied that reduction in the extent of Arctic sea ice in the summer weakens the upper-level zonal winds and triggers a polar-shifted jet stream. Therefore, the questions of whether summer UB activity is associated with Arctic sea ice changes, and if so, what the corresponding physical mechanisms are, naturally arise.

Many studies have presented evidence that links summertime circulation anomalies with preceding land surface conditions in mid-latitude regions; for example, Eurasian snow cover (Liu and Yanai, 2002) and soil moisture (SM; Ferranti and Viterbo, 2006; Fischer *et al*., 2007; Zampieri *et al*., 2009; Miralles *et al*., 2014) in spring are thought to excite significant wave trains that are accompanied by intensified UB. These surface condition anomalies are generally determined by precipitation changes, which may result from decreases in autumn Arctic sea ice (Honda *et al*., 2009; Bader *et al*., 2011; Liu *et al*., 2012; Li and Wang, 2014). Considering these previous findings, this study also focuses on evidence that links Arctic sea ice with changes in land surface conditions that thermodynamically favour the occurrence of summertime UB events.

To address these questions, we compare observations and the results of atmospheric circulation model experiments in the present study to better understand the summertime mid-latitude atmospheric responses to Arctic sea ice changes; further, we identify the potential dynamic and thermodynamic mechanisms. The subsequent sections of the paper are organized as follows. The data sets, methodologies, and numerical model used are described in section 2. The inter-annual variation in UB activity and its relationship with Arctic sea ice are investigated in section 3. In section 4, we explore the associated possible mechanisms. section 5 presents the responses of UB activity to changes in Arctic sea ice based on numerical experiments performed using the CAM5.0 model. A discussion and a summary are provided in the last section.

2 | THE DATA, METHODS, AND NUMERICAL MODEL

2.1 | Data

The data sets analysed in this study include (a) the monthly and daily mean geopotential height, wind, and air

temperature fields at various levels extracted from the National Centers for Environmental Prediction/National Center for Atmospheric Research (NCEP/NCAR) Reanalysis I (Kalnay *et al*., 1996); (b) the monthly mean Hadley Centre sea ice concentration (SIC) and sea surface temperature (SST) data set (referred to as HadISST; Rayner *et al*., 2003); (c) the monthly mean SM from 1979 to 2013 extracted from the ERA-Interim reanalysis, which has a horizontal resolution of 0.75 × 0.75° and four vertical levels at depths of 7, 21, 100, and 289 cm, respectively (Balsamo *et al*., 2009); and (d) the daily mean NOAA Climate Prediction Center (CPC/NOAA) global land surface precipitation data set, which has a spatial resolution of 0.5 × 0.5° (Xie *et al*., 2007).

2.2 | UB frequency

To investigate the potential association between the inter-annual variations in summer UB and the Arctic SIC, the blocking events over the Ural region were identified by Tibaldi and Molteni (1990), who considered the daily 500-hPa geopotential height (Z500) gradient over a longitudinal extent of 40°–80°E. As suggested by Cheung and Zhou (2015) and Luo *et al*. (2016a; 2016b), four major steps are involved in extracting the blocking events and thus defining the UB frequency index (UBI):

Step 1: The Z500 gradients, northern gradients between (80°N + Δ) and (60°N + Δ) and southern gradients between (60°N + Δ) and (40°N + Δ) at a given longitude are used to determine whether the flow is zonal or meridional; here, Δ is −5°, 0, 5°.

Step 2: A longitude is considered to be blocking if the northern gradients $(Z_{80°N+\Delta} - Z_{60°N+\Delta})/(80°N + \Delta - (60°N + \Delta)) \leq -10$ gpm/latitude and the southern gradients $(Z_{60°N+\Delta} - Z_{40°N+\Delta})/(60°N + \Delta - (40°N + \Delta)) \geq 0$ for at least one of the three values of Δ. Considering the characteristic timescale of blocking events, an identified blocking event should have a duration of at least five consecutive days.

Step 3: A UB event is identified when the large-scale circulation condition in step 2 is satisfied, the mean positive height anomaly is centred over 40°–80°E over the lifetime of the event, and the onset date of the event is in the summer (JJA; Luo *et al*., 2016a).

Step 4: The UBI is defined as the JJA-mean blocking frequency averaged over 40°–80°E in each summer. Note that, in this study, UB and the UBI refer to the JJA mean; other seasons are not discussed.

As we focus on inter-annual variations, the linear trend in the UBI is removed after the blocking event detection is carried out, and the linear trends in the other variables are also removed. The seasonal mean anomalies are given relative to the means for the entire period analysed here. Composite and regression analyses are adopted in the present study to diagnose the association between SIC and the mid- to high-latitude circulation anomalies. The composite differences and regression coefficients are considered to be robust when they are statistically significant at the 90 and 95% levels, based on two-sided Student's *t* tests. The effective number of degrees of freedom is calculated following Davis (1976).

2.3 | The Eady growth rate

The Eady growth rate (EGR) is employed as a measure of atmospheric baroclinicity, which reflects the characteristics of basic flow baroclinicity (Lindzen and Farrell, 1980). The EGR is defined as

$$\sigma = 0.31 \frac{f}{N} \frac{du}{dz}, \tag{1}$$

where 0.31 is a non-dimensional coefficient; f is the Coriolis parameter; N is the constant Brunt–Vaisala frequency; u is the zonal wind; and Z is the height. Hoskins and Valdes (1990) have indicated that the EGR is properly calculated above the boundary layer, where N is not dominant. Therefore, to avoid poor estimates of the EGR, the EGR of the lower troposphere (700 hPa) is calculated in the present study.

2.4 | Synoptic-scale transient eddy activity and eddy-vorticity forcing

Following Lau and Holopainen (1984), the synoptic-scale transient eddy activity (STEA) is estimated using the root-mean-square of the 2–8-day Lanczos bandpass-filtered Z500 (Duchon, 1979).

The synoptic eddy-vorticity forcing is important in maintaining low-frequency flow over the mid-latitudes (Kug and Jin, 2009; Ren *et al*., 2009). In the present study, the role of synoptic transient eddy-vorticity forcing associated with Arctic sea ice anomalies is investigated. Following Lau and Holopainen (1984), the synoptic transient eddy-vorticity forcing is represented by the stream function tendency (SFT), which is obtained by solving the Poisson equation:

$$\nabla^2 \mathrm{SFT} = -\nabla \overline{V'\zeta'}, \tag{2}$$

where V' and ζ' are the synoptic eddy components of the horizontal wind vector and the relative vorticity, respectively, which are calculated by 2–8-day Lanczos bandpass filtering of the relevant fields. It should be noted that only the SFT associated with the synoptic transient eddy-vorticity fluxes is considered and not the total SFT.

2.5 | Numerical model

Version 5.0 of the Community Atmospheric Model (CAM5.0) distributed by NCAR is applied to explore the impacts of Arctic SICs on the inter-annual variations in summer UB activity. CAM5.0, the atmospheric component of the Community Earth System Model (CESM), is coupled to

the Community Land Model (CLM); thus, the SICs and SSTs must be prescribed. In this study, each grid cell has dimensions of 1.9° latitude × 2.5° longitude, and the model includes 30 vertical levels; the top level is located at 3.6 hPa. One of the improvements featured in this version of the model is that it displays a realistic seasonal cycle of Arctic clouds, which are essential in reflecting the response of the Arctic to increases in greenhouse gases (Kay *et al*., 2012).

3 | THE INTER-ANNUAL VARIATIONS IN SUMMER UB AND ITS ASSOCIATION WITH ARCTIC SEA ICE

Figure 1a shows the normalized JJA UBI from 1980 to 2013 determined from the NCEP/NCAR reanalysis. The UBI displays clear inter-annual variability, and no significant trend is noted for this period. Figure 1b displays JJA-mean Z500 anomalies regressed against the UBI. A pronounced mid-latitude wave train pattern is observed across the North Atlantic and the Eurasian continent, with positive height anomalies over the North Atlantic and the Ural Mountains and negative height anomalies over the Greenland–Barents Seas and Lake Baikal; these results are consistent with those described by Wu *et al*. (2013) and Petrie *et al*. (2015). The prominent anticyclonic anomaly over the Ural Mountains associated with this wave train may favour the frequent occurrence of summer UB activity. In a vertical cross section of the geopotential height anomalies along 60°N, this wave train exhibits a quasi-barotropic structure and a deep blocking-type ridge over the Ural Mountains (Figure 1c). In contrast, the opposite features would occur in low-UBI years.

To investigate the association of Arctic SICs with summer UB variation, it is essential to examine whether SIC

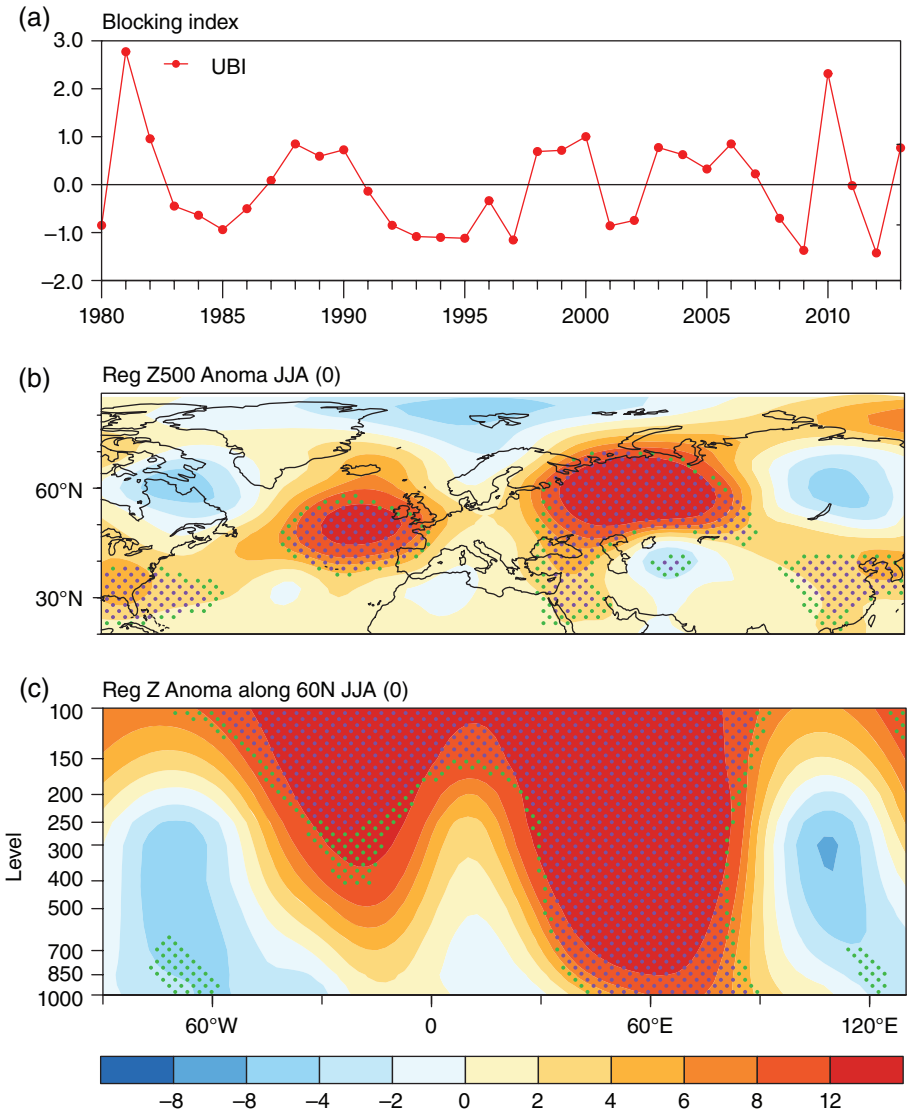

FIGURE 1 (a) The normalized summer (JJA) Ural blocking event frequency index (UBI) for the period of 1980–2013. (b) The JJA Z500 anomaly and (c) a vertical cross section of the geopotential height anomaly along 60°N regressed against the JJA UBI. Values that significantly exceed the 90 and 95% confidence levels are indicated by green and purple dots, respectively

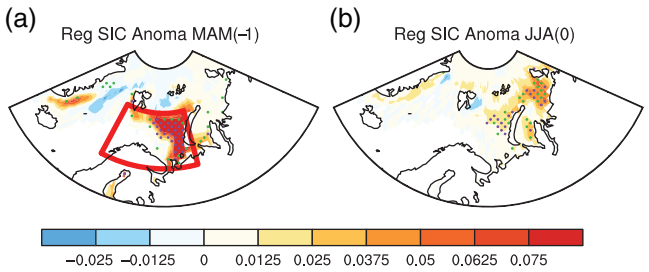

FIGURE 2 (a) MAM and (b) JJA Arctic SIC anomalies regressed against the JJA UBI. The red sector in (a) denotes the region 67°–77°N, 10°–56°E, in which the MAM SICI is defined. Values that significantly exceed the 90 and 95% confidence levels are indicated by green and purple dots, respectively. In the titles, (−1) denotes the preceding season, whereas (0) denotes the present summer

anomalies are linked to this North Atlantic–Eurasian wave train. Figure 2 shows the Arctic SIC anomalies from the preceding spring to the following summer, regressed against the UBI. During the spring, statistically significant heavy SICs are detected over the Atlantic sector that extends from the Greenland Sea to the Barents Sea, together with light SICs in Baffin Bay (Figure 2a). During the following summer, a similar but relatively weak positive anomaly persists in the Barents–Kara Seas (Figure 2b). These continuously heavy Arctic SICs over the region from the Norwegian Sea to the Barents Sea could lead to a locally anomalous weak low at 500 hPa; this is mainly due to its cooling effect on air volume, which reduces mid-tropospheric geopotential heights in ways similar to the results in a previous study (Peings and Magnusdottir, 2014). This anomalous low is along with an anomalous wave train pattern excited remotely over the mid-high latitudes in summer (figure omitted), consistent with the wave train pattern regressed against the UBI illustrated in Figure 1.

According to Alexander *et al*. (2004), an increase in the Arctic SIC may cause decreased upwards surface heat fluxes and near-surface cooling. To investigate the heat flux responses to Arctic sea ice variability, we define a spring SIC index (SICI) as the regional average SIC over the Barents Sea (67°–77°N, 10°–56°E), where the anomalous signals are particularly significant. Figure 3 compares the regression anomalies of the surface turbulent heat flux from spring to summer against the JJA UBI and the MAM SICI. The heat flux patterns obtained by regression against the JJA UBI are characterized by negative anomalies over the zonal belt-like regions in proximity to areas of ice expansion, and these anomalies contribute to strong local cooling. Meanwhile, a significantly positive heat flux anomaly emerges over the Ural region in summer (Figure 3a,b), which may serve as a forcing on the development of UB. As indicated by previous studies, drier soil-induced heat fluxes favour local warming to dry air masses, which decreases convection and increases boundary layer height and the development of upper-air anticyclonic circulation (Zampieri *et al*., 2009; Miralles *et al*., 2014). The heat fluxes associated with heavy SICs exhibit a similar spatial distribution of the surface turbulent heat fluxes over the Barents Sea and the Ural Mountains (Figure 3c,d) as those in Figure 3a,b.

Therefore, the statistically significant relationship between the continuous heavy (light) SICs within the Barents Sea from spring to summer and the mid-latitude wave train may provide a linkage to the frequent (rare) occurrence of summer UB activity. In the following sections, we will explore the possible underlying dynamic and thermodynamic mechanisms.

4 | POSSIBLE PHYSICAL MECHANISMS

4.1 | The role of the westerly jet stream

In winter, weakened westerly winds in mid-latitude regions are typically associated with an increase in atmospheric blocking events (Newson, 1973) and slower eastwards progression of Rossby waves in the Northern Hemisphere (Palmén and Newton, 1969). Recently, Hassanzadeh *et al*. (2014) and Hassanzadeh and Kuang (2015) have indicated that the reduction in near-surface mid-latitude to polar temperature differences caused by Arctic amplification would increase blocking events by slowing down the mid-latitude westerly wind. Luo *et al*. (2016a; 2017) provided further observational evidence suggesting that losses of sea ice in the Barents–Kara Seas would lead to persistent UB activity through slowing the westerly wind in winter. However, compared to the winter season, the response of summer mid-latitude westerly winds to anomalous SIC conditions have received less attention. Thus, we propose the hypothesis that the changes in mid-latitude westerly winds driven by Arctic SICs may increase the probability of UB events in summer.

Figure 4 compares the regression anomalies of the JJA mean 500-hPa zonal wind (U500) against the JJA UBI and the MAM SICI. The climatological U500 displays two large positive centres over Eurasian mid to high latitudes: high-latitudes over the Northern Europe–Barents Sea region and mid-latitudes over the Caspian Sea–East Asia region. As the number of UB days increases and the SICs increase, it can be seen that the U500 increases in strength over the former centre but is particularly weak over the latter centre (especially for UB regions) in both patterns (Figure 4a vs. Figure 4d). Note that Figure 4d reveals a southeastwards shift in the positive anomaly centre relative to that in Figure 4a, which may be due to the MAM SIC-induced heat flux anomaly that is restricted over the southern region of the Barents Sea. To some extent, the meridional dipole of U500 stretching across the mid- to high-latitudes provides a background against which blocking events occur and thereby encourages the development or persistence of blocking events over the Ural Mountains. As suggested by previous research (Williams *et al*., 2007; Francis and Vavrus, 2012; Hassanzadeh *et al*., 2014),

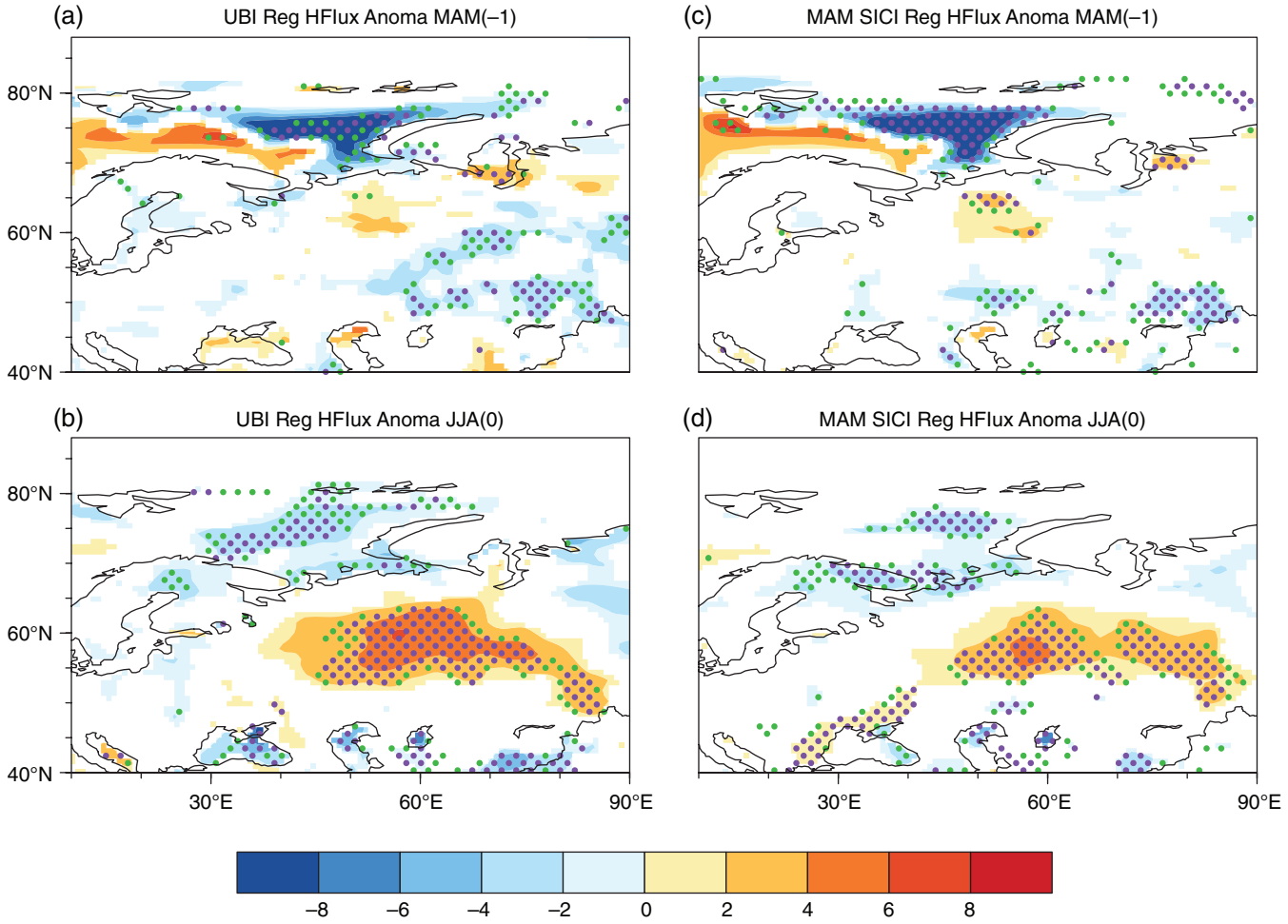

FIGURE 3 (a) MAM and (b) JJA surface heat flux (sensible + latent) anomalies regressed against the JJA UBI. (c, d) Same as in (a, b) but regressed against the MAM SICI. Values that significantly exceed the 90 and 95% confidence levels are indicated by green and purple dots, respectively

changes in zonal winds are largely determined by the localized MTG and eddy-forcing anomalies in the lower troposphere. Given that the distribution of anomalous SICs and the associated subsequent changes in snow cover on the Eurasian continent (Liu *et al*., 2012) may modulate the polewards temperature gradient, we show in Figure 4b,e the spatial patterns of the 700-hPa MTG over the middle to high latitudes. The heavy SICs condition corresponds to strong and persistent Arctic cooling over the Barents Sea from spring to summer, which forces the MTG to increase over the regions north of 60°N and south of the northern Barents Sea. A similar southeastwards shift in the positive MTG anomaly is also detected in Figure 4e relative to that in Figure 4b. This result essentially illustrates that the southeastwards movement of the U500 is largely affected by the movement of the MTG. Moreover, the increase in UB-related U500 at high latitudes may also be affected by other factors, such as the SM located south of this high-latitude region (Francis and Vavrus, 2012); this will be discussed in the following section. The differential surface thermal condition of the Arctic relative to the mid-latitude regions is the key link between the Arctic sea ice anomalies and circulation patterns and favours the persistence of blocking events in mid-latitude regions.

To clearly display the evolution of the MTG and U500 anomalies from April–June (AMJ) to JJA, Figure 4c,f show the 3-month evolution of average anomalies for MTG and U500 over high-latitude regions extending northwards from northern Europe to the Barents Sea (60°–77°N, 20°–70°E) and mid-latitude regions over the Ural Mountains (40°–55°N, 40°–80°E). The high-latitude MTG and U500 indices both reveal progressively increasing trends with maximum amplitudes occurring in JJA, whereas the mid-latitude U500 index shows decreasing trend. These trends are similar to those identified in previous studies (Butler *et al*., 2010; Cohen *et al*., 2013). These results imply that the MTG increase related to heavy SICs may modulate the mid- to high-latitude U500s that likely contribute to the increased frequency of UB events in summer. In addition, the previous studies also support this idea: the weaker westerly winds over Eurasian mid-latitudes surrounding the UB regions are associated with increased atmospheric blocking events in the Northern Hemisphere (Barriopedro and Garcia-Herrera, 2006).

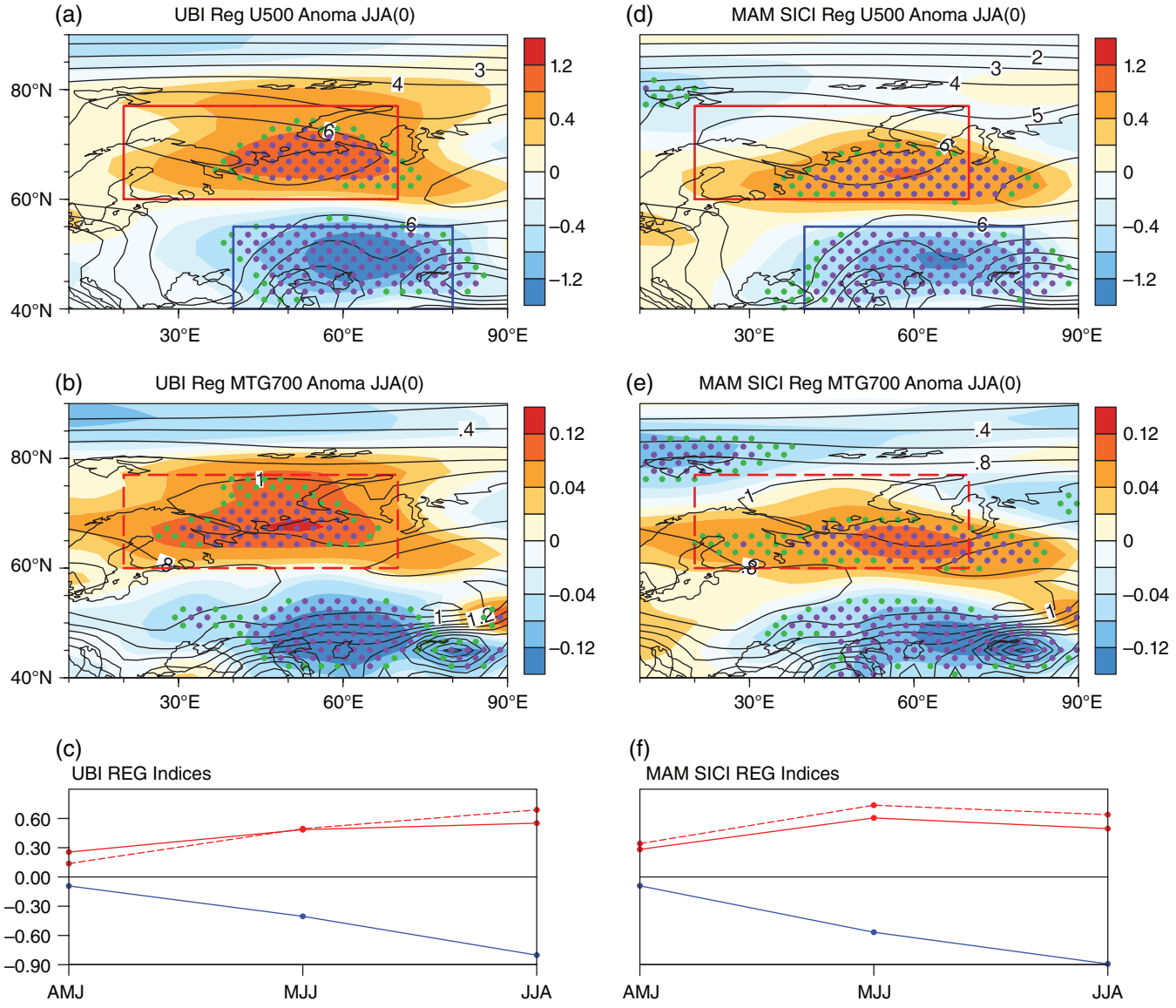

FIGURE 4 (a) JJA 500-hPa zonal wind and (b) 700-hPa MTG anomalies regressed against the JJA UBI (shadings) and their climatology (contours). (c) The 3-month running mean evolution of the high-latitude zonal wind (solid red line) and MTG (dotted red line; multiplied by 10) anomaly indices and the mid-latitude zonal wind (blue line) anomaly index from the preceding AMJ to the following JJA. These high-latitude indices are defined as average anomalies over the red sector (60°–77°N, 20°–70°E), whereas the mid-latitude index is defined over the blue sector (40°–55°N, 40°–80°E). (d–f) Same as in (a–c) but regressed against the MAM SICI. Values that significantly exceed the 90 and 95% confidence levels are indicated by green and purple dots, respectively

4.2 | The role of STEA

In this section, we investigate how Arctic SICs affect UB activity by adjusting the synoptic transient eddies in the mid-latitude regions. As many studies have reported, upstream eddy-vorticity forcing plays a key role in the establishment of blocking through the advection of low potential vorticity air from the subtropics (Nakamura and Wallace, 1993). These eddies also tend to maintain blocking events through eddy straining; when eddies propagate along jets and encounter a ridge, they become elongated in the meridional direction and provide vorticity for the blocking (Shutts, 1983). Thus, we investigate whether heavy (light) SICs drive variations in summer UB frequency by producing changes in synoptic transient eddies.

In Figure 5, we primarily analyse the climatological distributions of the 700-hPa EGR, STEA and synoptic eddy-vorticity forcing (SFT) at 500 hPa (see section 2) and regression anomalies against the JJA UBI and MAM SICI. The climatological EGR displays two similarly large centres that are collocated with those for U500 and MTG. The increased UB frequency corresponds to an enhanced (reduced) low-level EGR to the south (north) of the region of heavy SICs that is marked as location A (B) in Figure 5a. Another negative centre can also be seen in the regions surrounding the Ural Mountains (location C). This EGR pattern largely resembles the MTG pattern (Figure 4b), indicating that the MTG and EGR anomalies are closely related. The increased lower tropospheric

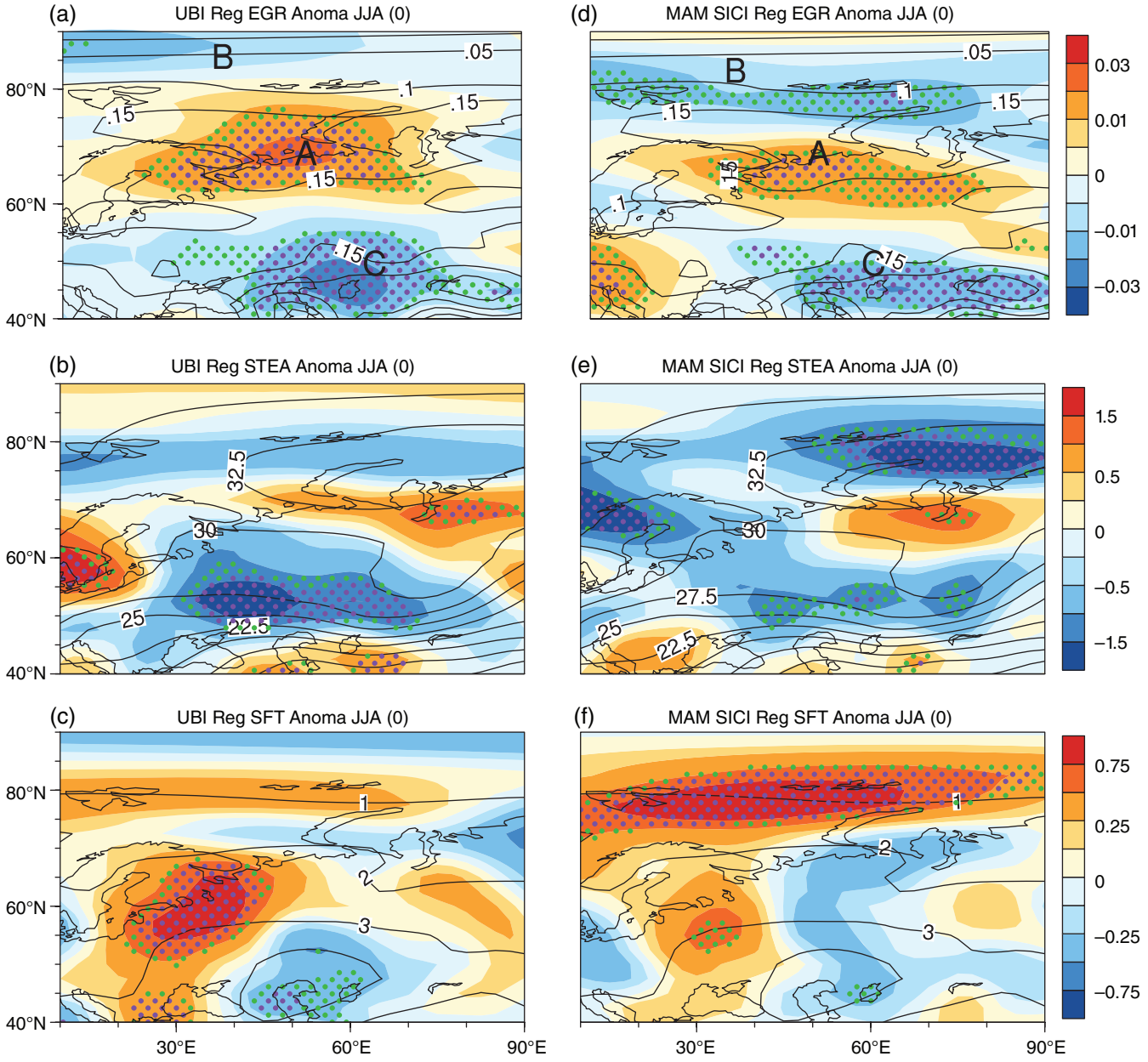

FIGURE 5 (a) JJA 700-hPa EGR, (b) 500-hPa STEA, and (c) 500-hPa SFT anomalies regressed against the JJA UBI (shadings) and their climatology (contours). (d–f) Same as in (a–c) but regressed against the MAM SICI. The letters A (B and C) denote the regions with enhanced (decreased) low-level baroclinicity. Values that significantly exceed the 90 and 95% confidence levels are indicated by green and purple dots, respectively

baroclinicity in location A favours additional transient eddy activity (Fang and Yang, 2016). An apparent negative anomaly of STEA is found in regions extending from the East Europe Plateau to the Ural Mountains and positive anomalies extending along the zonal belt from northern Europe to south of the area of heavy SICs; this pattern reflects a northwards displacement relative to climatological conditions (Figure 5b). This weakened STEA may lead to local intensification of eddy-vorticity forcing (Hoskins *et al*., 1983). In Figure 5c, we show the regression anomaly of the 500-hPa SFT against the UBI index, and a rather distinct increase in the SFT can be seen over the East Europe Plateau. This eddy forcing is expected to drive downstream UB events, as suggested by Luo *et al*. (2016b; 2017) which presented evidence indicating that upstream synoptic eddies in Europe influence downstream blocking events. However, the large SFT centre near the Caspian Sea is weakened, which implies a greater impact from upstream forcing than that from localized forcing. To a certain degree, similar responses can also be found for heavy SIC conditions (Figure 5d–f). However, when compared with Figure 5a, the positive EGR centre over location A tends to move southeastwards (Figure 5d), and relatively weaker STEAs and SFTs are also detected over Eurasian mid-latitudes (Figure 5e,f), which may also be affected by the same factors that affect the MTG and U500 fields.

4.3 | The thermodynamic effects of Eurasian SM

In addition to direct dynamical processes of the westerly jet stream and STEA, summer UB may also be affected by anomalous Eurasian SM conditions through thermodynamic processes (Ferranti and Viterbo, 2006; Fischer *et al*., 2007; Zampieri *et al*., 2009; Miralles *et al*., 2014). According to previous studies (Liu *et al*., 2012; Cohen *et al*., 2013), the autumn Arctic SIC retreat may lead to excessive Eurasian snowfall in winter. We thus attempt to identify the corresponding cause–effect relationship in spring.

In Figure 6, we investigate the possible linkage between European precipitation anomalies in April–June with the spring SICs and summer UB, respectively. This feature implies that the enhanced springtime SIC may cause a deficit in precipitation in East Europe Plateau, i.e., the upstream region of the Ural Mountains, in late spring and early summer that is also related to increased UB frequency. The reduced precipitation is followed by anomalously low SM, integrated in the vertical levels from 0 to 289 cm at the mid- to high-latitudes in spring; during the summer, stronger signals are visible in over larger areas, as illustrated in Figure 7a,b. Correspondingly, higher surface sensible heat fluxes occur in the mid-latitude regions (Figure 7c,d); on the other hand, the robust heat flux centre shifts southwards relative to the negative SM centre, as snow cover and frozen soil typically melt faster at lower latitudes. These findings indicate that reduced precipitation in Europe appears to desiccate the underlying soil from AMJ to the following summer and therefore enhances the upwards sensible heat flux over the mid-latitude regions of Europe in summer.

A deeper knowledge of the mechanisms involved in the formation of UB events is necessary to quantify the importance of surface conditions. As noted by Zampieri *et al.* (2009), the knowledge of SM feedback is crucial. Next, we examine the possible effects of SM deficits on the East Europe Plateau on the mid-latitude circulation. We first define the previous AMJ season and the JJA-mean SM index (SMI) as the averaged SM anomalies within the region 54°–64°N, 42°–60°E (red rectangles in Figure 7a,b) and calculate their regression with the atmospheric thickness (Z500–Z1000) and the 500-hPa geopotential height. The regression pattern of JJA circulation field with the AMJ SMI reveals a prominent positive height (thickness) anomaly and an anomalous anticyclone over the Ural Mountains, which is associated with a significant wave train that prevails over the mid- to high-latitude regions of the Atlantic–Eurasian continent (Figure 8a,b). We also find circulation features influenced by the JJA SMI (Figure 8c,d) are similar to those influenced by the AMJ SMI. The features mentioned above generally resemble the circulation associated with UB activity (Figure 1b). Therefore, the effects of continuous AMJ–JJA soil conditions on summertime UB are as anticipated: dry soil causes higher heat fluxes and enhanced mid-latitude warming, contributing to the amplification of atmospheric thickness and Z500 over the Ural Mountains.

From a physical point of view, the dynamic and thermodynamic effects of Arctic SICs may be synergistic and dependent. In Table 1, we show the statistical relationship between the normalized historical series of the MAM SICI and the JJA SMI, which indicates a negative correlation coefficient of −0.40. This result suggests that precipitation changes and subsequent changes in SM may also be determined by SIC-induced physical processes. Regression analyses of SM anomalies against the U500 and STEA indices (figures omitted) have validated this hypothesis.

4.4 | The combined effects of the Arctic SIC and Eurasian SM

The combined effects of Arctic SICs during the preceding MAM and the simultaneous JJA Eurasian SM on summer UB are further explored in this section using composite analysis. Before displaying the results of this investigation, we examined the relationships among the normalized historical series of the MAM SICI, the JJA SMI, and the JJA UBI in Table 1. The JJA UBI is positively correlated with the MAM SICI (0.46), and is positively correlated with the JJA SMI

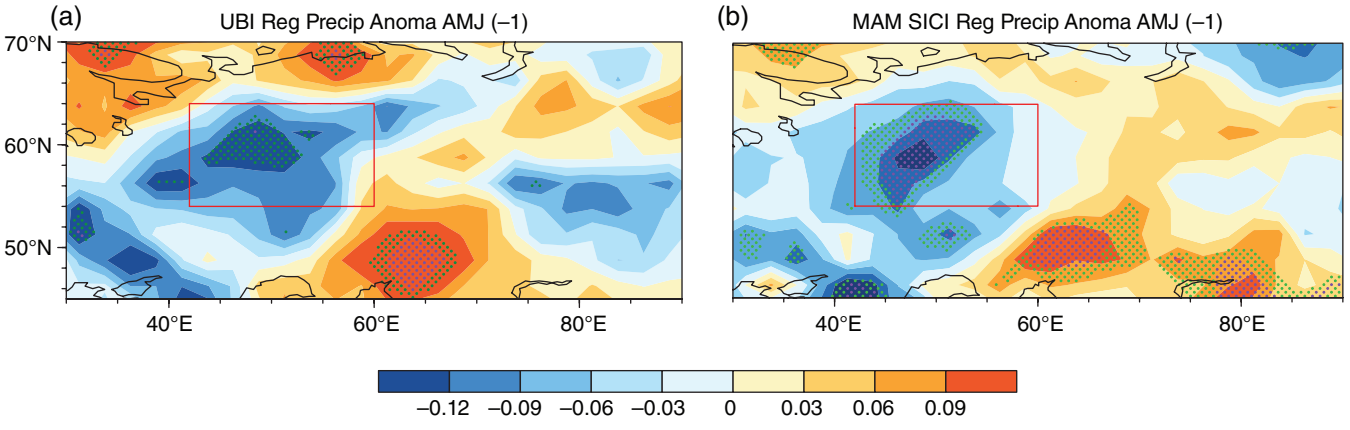

FIGURE 6 April–June mean European precipitation anomalies regressed against the (a) JJA UBI and (b) MAM SICI. Values that significantly exceed the 90 and 95% confidence levels are indicated by green and purple dots, respectively

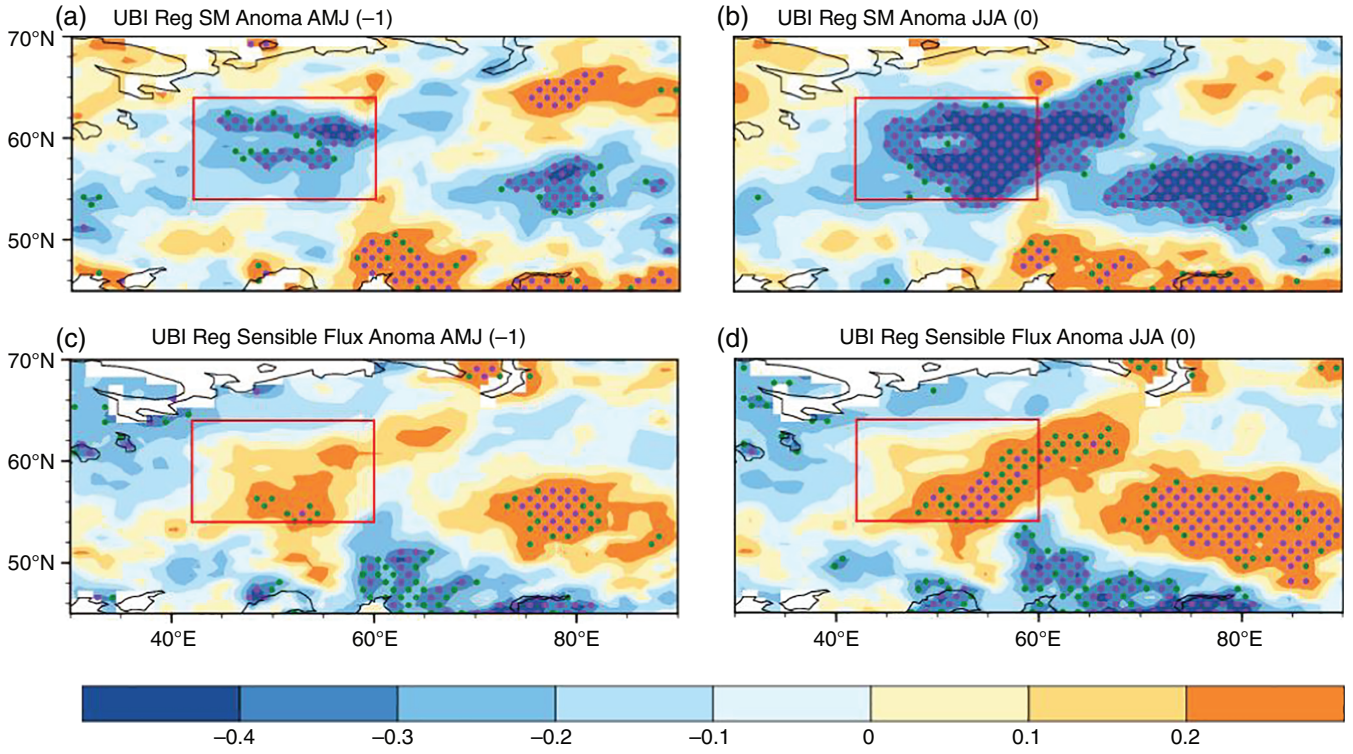

FIGURE 7 (a) AMJ and (b) JJA SM anomalies regressed against the JJA UBI. (c, d) Same as in (a, b), except that surface sensible flux anomalies are considered. The red rectangle in (a, b) denotes the region 54°–64°N, 42°–60°E, in which the AMJ and JJA SM indices are defined. Values that significantly exceed the 90 and 95% confidence levels are indicated by green and purple dots, respectively

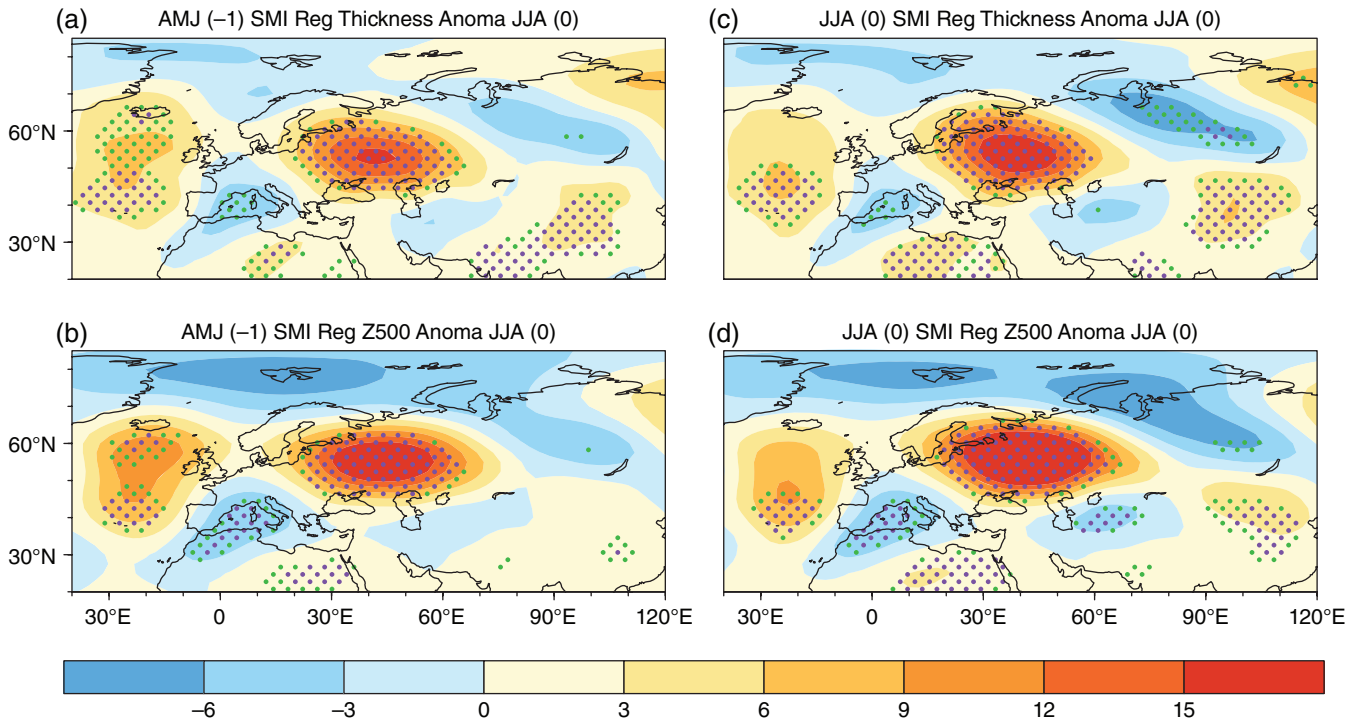

FIGURE 8 (a) JJA low-middle tropospheric thickness (Z500–Z1000) and (b) Z500 anomalies regressed against the AMJ SM index (SMI). (c, d) Same as in (a, b) but regressed against the JJA SMI. Values that significantly exceed the 90 and 95% confidence levels are indicated by green and purple dots, respectively

(−0.46), both of these correlation coefficients exceed the 95% confidence levels. The above cross-correlation coefficients indicate that the combined influence of anomalies in the MAM SICs and the JJA SM in Eurasia on summer UB events must also be considered, as it may produce an asymmetrical response of mid-latitude circulation patterns.

Figure 9 compares the composite circulation differences for different phase combinations of the MAM SIC and JJA SM

TABLE 1 Correlation coefficients between the MAM SICI, JJA SMI, and JJA UBI

	SICI	SMI
UBI	0.46	−0.46
SICI		−0.40

anomalies for summertime Z500 over the Atlantic–Eurasian regions. First, we define heavy/light SICs and SMs conditions with a criterion of ±0.2 *SD* for both indices; for significantly heavy/light SICs and SMs conditions, a criterion of ±0.5 *SD* are utilized. In years that feature heavy SICs in MAM and dry soil in JJA (12 years; Figure 9a), a significant positive height anomaly is seen in the Ural region and largely projects the spatial pattern that is regressed against the UBI. In contrast, Z500 presents an opposite (negative) anomaly over the Ural Mountains in years that feature light SICs in MAM and wet soil conditions in JJA (11 years; Figure 9b). Furthermore, in years that feature significantly heavy SICs in MAM and dry soil conditions in JJA (4 years; Figure 9c) and significantly light SICs in MAM and wet soil conditions in JJA (6 years; Figure 9d), the Z500 anomalies become especially pronounced, which sheds light on the hypothesis that the combined effects of these features may reinforce the Z500 response. On the other hand, when the changes in the MAM SICs are opposite to those in SMs in JJA (e.g., heavy SICs but wet soil conditions, as occurs in 6 years; Figure 9e), Z500 exhibits a positive but relatively weak anomaly over the Ural Mountains. For light SICs and dry soil conditions (6 years; Figure 9f), negative height anomalies appear over the Ural Mountains. This result may imply that heavy SICs and wet SMs seem to offset their individual effects, as well as the light SICs and dry SMs. The response of Z500 is predominantly determined by the changes in Arctic SICs. These analyses suggest the importance of the combined effects of SICs and soil conditions in affecting atmospheric circulation patterns in mid- to high-latitude regions and suggest the aforementioned synergistic dependence between the dynamic and thermodynamic effects of Arctic SICs.

5 | MODEL SIMULATIONS

5.1 | Experimental design

This section describes numerical simulations conducted to assess the large-scale atmospheric responses that occur at mid- to high-latitudes by imposing two different Arctic SIC conditions, specifically heavy and light Arctic SICs, using the CAM5.0 model. The control run is a 60-year simulation with prescribed annually repeating SSTs and SICs, which represents the overall climatology for the 1980–2013 period, and the first 10-year are discarded for spin up. Two

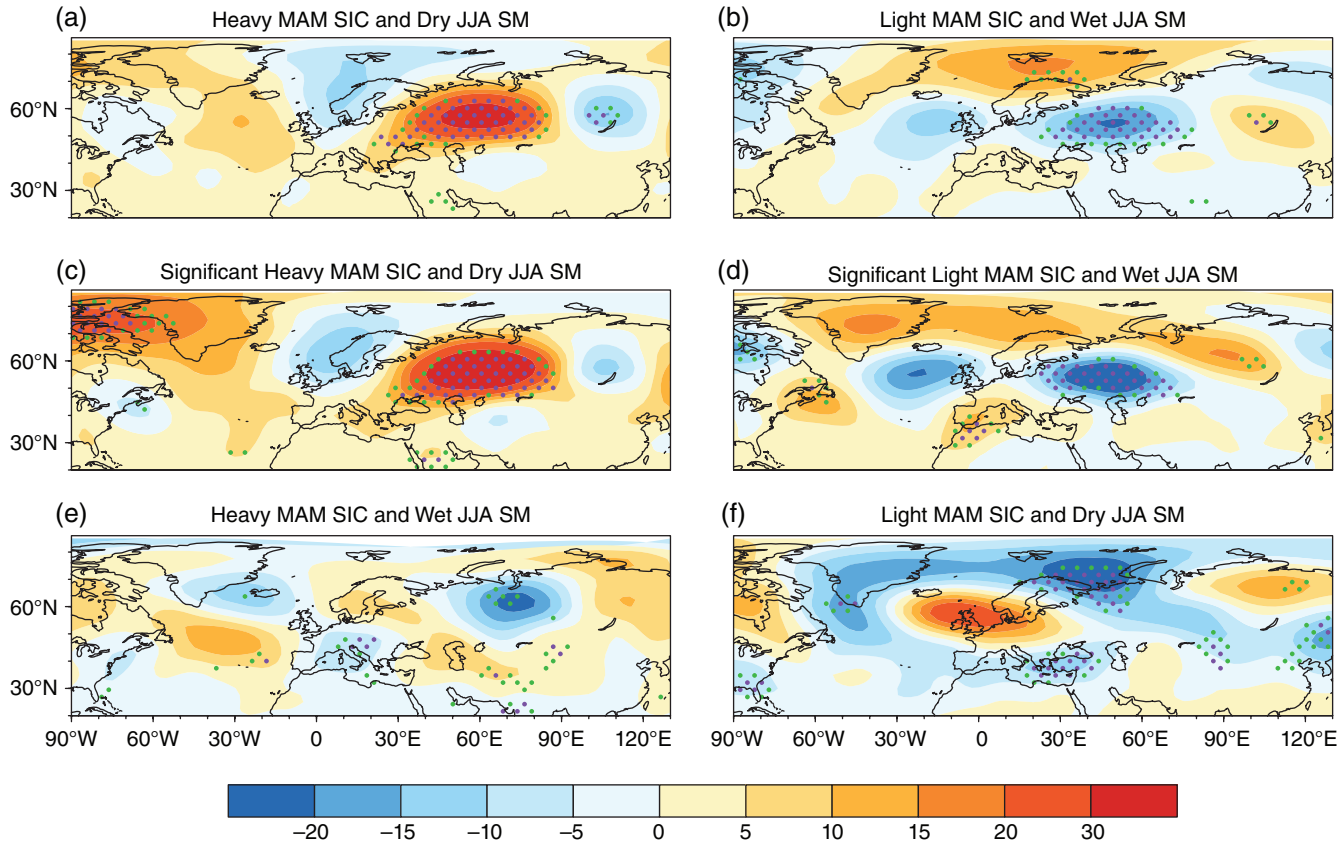

FIGURE 9 Composite differences in JJA Z500 in (a) heavy MAM SIC and dry JJA soil years, (b) light MAM SIC and wet JJA soil years. (c, d) Same as in (a, b), except that significant years are considered. (e) Heavy MAM SIC and wet JJA soil years, and (f) light MAM SIC and dry JJA soil years. Values that significantly exceed the 90 and 95% confidence levels are indicated by green and purple dots, respectively

perturbation experiments (i.e., the heavy SIC and light SIC experiments) are paired with the control run; these experiments differ only in terms of their SIC and SST boundary conditions. The mid- to high-latitude atmospheric response in the model is estimated as the ensemble mean difference between the heavy SIC and light SIC experiments.

Detailed information on the experimental design is provided in Table 2. Annually repeating cycles of SICs and SSTs are prescribed as the boundary conditions in these runs. In the heavy SIC experiment, the prescribed monthly SIC annual cycle employed in the model is computed using the HadISST data set. The monthly Arctic SICs anomalies during the 1980–2013 period over the region 67°–88°N, 20°W–70°E (shown in Figure 2), which are obtained by regression against the JJA UBI index, are added to the prescribed climatology from March to August; similarly, monthly SSTs are changed in regions where the SICs have changed substantially to include the coherent SST effects associated with SIC changes. Based on Peings and Magnusdottir (2014), if the Arctic SIC anomalies exceed by 10% or more, the SST anomalies obtained by the regression on the JJA UBI are added to the SST climatology of the corresponding month. Thus, only the changes in the SICs and SSTs associated with the SICs changes are considered. Otherwise, Arctic SICs and SSTs from September to the following February are set to the climatological values, which are exactly the same as those in the control simulation. For the light SIC experiments, the polarities of the SIC and SST anomalies are opposite to those seen in the heavy SIC experiments, consistent with light SIC conditions.

A large number of ensemble members (50–60 or more) is required to confidently detect the mid- to high-latitude responses to Arctic sea ice changes (Screen *et al*., 2013a). In the present study, for each experiment, 50 members were integrated from December 1 to the following August 31 with different atmospheric initial conditions derived from a control run. Similar to Mori *et al*. (2014), the 50 initial members were selected from the 50-year mean state of the control run with 6-hr lags (e.g., 00Z01DEC, 06Z01DEC, etc.).

TABLE 2 Experimental designs used with CAM5.0

Experiments			Integration period
Perturbation	HSIC	SIC: The regressed monthly anomalies of Arctic SIC over the region (67°–88°N, 20°W–70°E) + prescribed SIC climatology SST: The regressed monthly anomalies of Arctic SST where SIC has substantially changed + prescribed SST climatology	12.1–8.31 50 ensemble members
	LSIC	SIC and SST anomalies opposite to the HSIC + corresponding prescribed climatology	
Control		Prescribed monthly SIC and SST climatologies	50 years

5.2 | Model results

To examine the summertime UB response to the forcing produced by anomalous Arctic sea ice conditions, we primarily assess the composite difference in the UBI between the heavy and light SIC experiments. Figure 10 displays a histogram representing UBI values from a 50-member ensemble and the associated anomalous percentage relative to climatological conditions. 30 of the 50 samples reproduce the positive difference in the UBI seen in the observations, and the largest UBI is as high as 4 days, with the anomalous percentage being 250%. On the other hand, 14 samples yield negative differences, and 6 samples reveal insignificant differences. These results indicate that the heavy SIC experiments produce more frequent UB activity than the light SIC experiments, reflecting the appreciable impacts of heavy SICs on the increased UB frequency in summer. In the following test, all 50 samples are utilized to analyse the atmospheric responses to the SIC differences at middle to high latitudes in the model.

Figure 11 shows the spatial distribution of the response in geopotential height in summer. A pronounced large-scale wave train in Z500 extends throughout the mid- to high-latitudes of Eurasia (Figure 11a) and is accompanied by a barotropic structure over the Ural Mountains in the vertical section along 60°N (Figure 11b). These height responses in the model are in agreement in terms of their geographic distribution with the observational results obtained by regression against the UBI index (Figure 1b,c); however, the amplitude of the model response is relatively small.

Figure 12 shows the summer large-scale circulation responses for U500, the surface air temperatures and the 700-hPa MTG and their climatology in the control run. During the spring, the positive U500 anomaly is located over the Arctic region and the mid-latitude region that extends from the Black Sea to Balkhash Lake, whereas the negative anomaly is located over northern Russia (Figure 12a). During summer, the climatological U500 in the control run is able to mimic the two large centres over the Eurasian mid- to high-latitude regions and is on the same order of magnitude as that in the observations. The positive U500 anomaly over the Arctic extends and shifts southwards to northern Russia, and the negative U500 anomaly begins to affect the mid-latitude region (Figure 12b), which agrees exactly with the observations (Figure 4a,d).

In spring (Figure 12c), extensive negative surface air temperature anomalies occur over regions extending from the Arctic to the continent; however, these anomalies are centred over the Barents Sea. In the following summer (Figure 12d), the negative temperature anomalies persist over the Arctic, whereas an apparent warming emerges over the western mid- to high-latitude part of the Eurasian continent. The related low-level MTG increases over the subpolar regions (Figure 12e,f), leading to a strengthening of localized U500 from the previous spring to the following

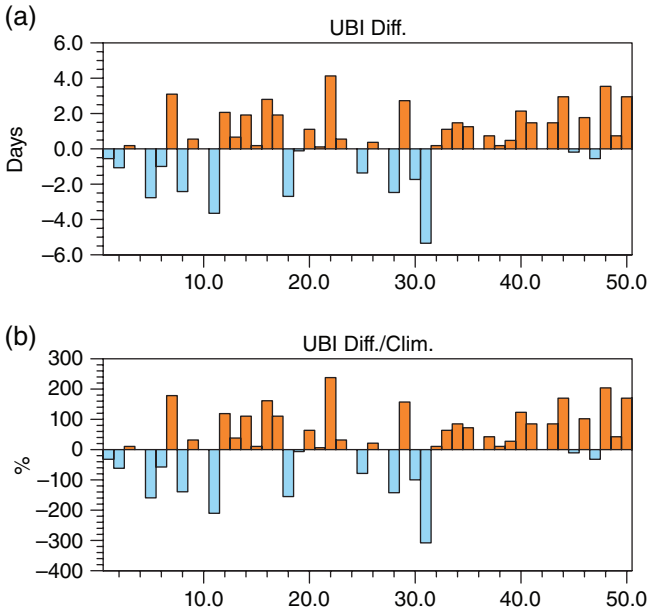

FIGURE 10 Histograms of the 50 samples of (a) UB frequency differences and the associated relative percentage differences between the heavy and light SIC experiments. Orange (blue) bars denote samples with higher (lower) frequencies

summer. The model reproduces the persistent increasing trends of the positive high-latitude MTG and U500 anomalies from AMJ to JJA seen in the observations (Figure 4e,f), as well as the continuous deceleration of mid-latitude U500 (Figure 13), which may contribute to intense UB activity.

To confirm the role of STEA in affecting the summertime UB, we show the model-simulated 700-hPa EGR, 500-hPa STEA and SFT in Figure 14. Their climatological distributions resemble those in the observations in terms of their spatial patterns and general order of magnitude. However, the climatological STEA seems to be weaker in high-latitude regions (Figure 14b); this bias may arise from the poor performance of CAM5 when simulating storm tracks (Gettelman *et al*., 2012). The heavy SICs correspond to a distinctly enhanced EGR to the south of the Barents Sea (location A) and decreased EGRs to the north (location B) and over the Ural Mountains (location C). Location A is essentially the same as that seen in the observations, as determined by regression against the UBI and SICI (Figure 5a,d). As the EGR increases at location A and decreases at location C, the STEA weakens accordingly over regions extending across eastern Europe and the Ural region (Figure 14b). Correspondingly, the intensified STEA-vorticity forcing is reproduced over the East Europe Plateau, which may influence the downstream region where most blocking events develop (Figure 14c). These simulations indicate the dynamic role of SIC-forced STEA in driving the downstream UB in summer, consistent with the observations.

Figure 15a highlights the European precipitation response in April–June, which is labelled reduced precipitation over the East Europe Plateau. Such a spatial distribution of precipitation desiccates the underlying soil and leads to continuous

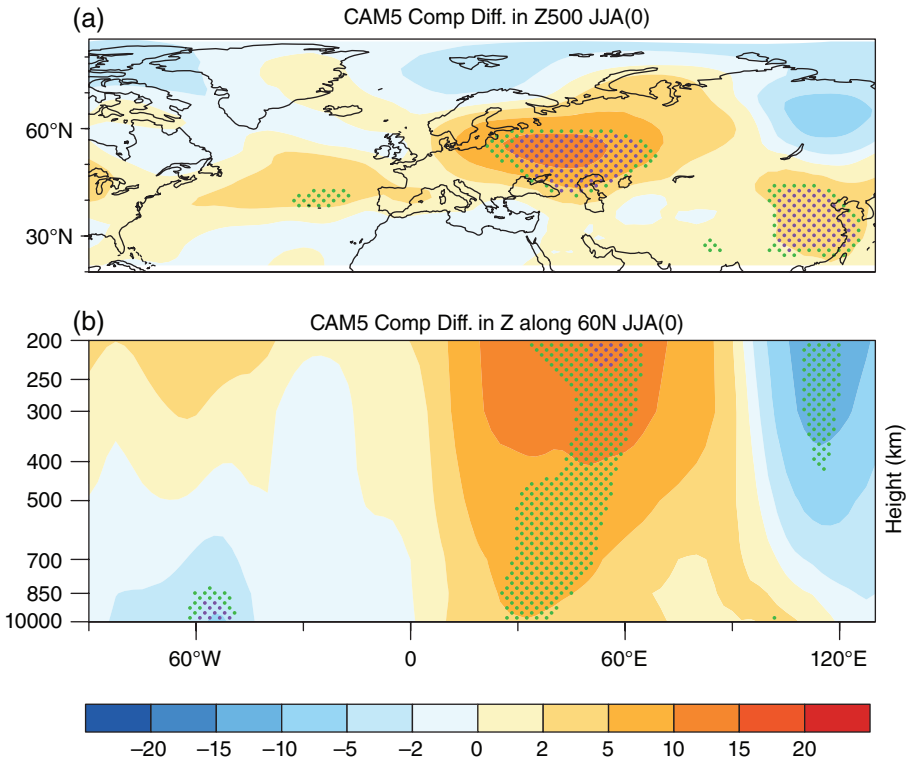

FIGURE 11 The simulated composite differences in the JJA (a) Z500 and (b) a vertical cross section of the geopotential height along 60°N between the heavy and light SIC experiments. Values that significantly exceed the 90 and 95% confidence levels are indicated by green and purple dots, respectively

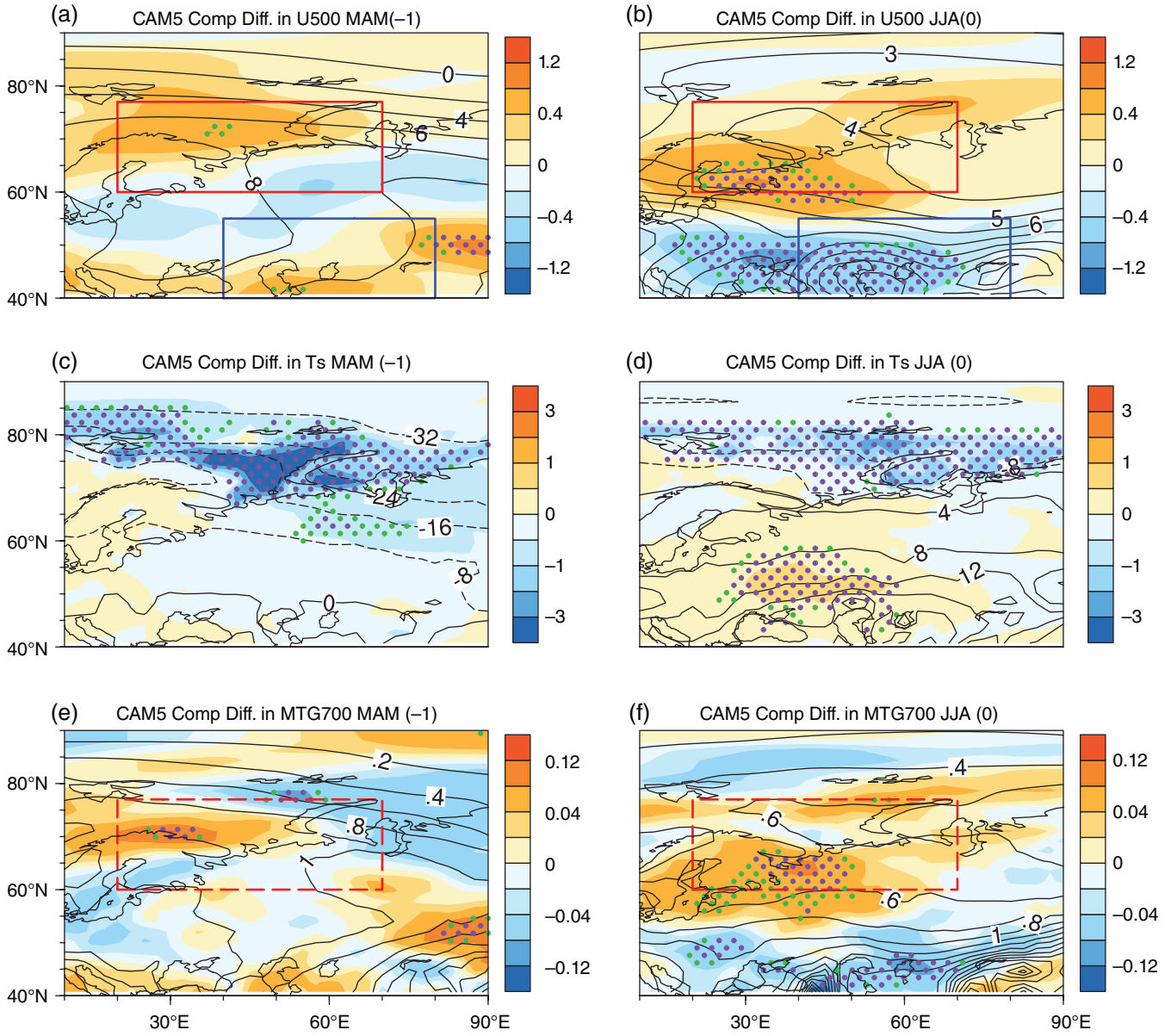

FIGURE 12 The simulated composite differences (shadings) in the (a) MAM and (b) JJA 500-hPa zonal winds between the heavy and light SIC experiments and their climatology in the control run (contours). (c–f) Same as in (a, b) except that air temperature and the 700-hPa MTG, respectively, are considered. Values that significantly exceed the 90 and 95% confidence levels are indicated by green and purple dots, respectively

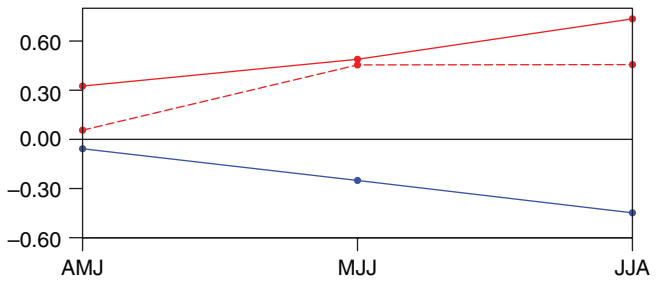

FIGURE 13 The simulated composite differences in the evolution of the 3-month running mean of the averaged high-latitude MTG (red dotted line, multiplied by 10) and zonal winds (red solid line) over the regions adjacent to the Barents Sea and the mid-latitude zonal winds (blue line) over the Ural Mountains between the heavy and light SIC experiments from the preceding AMJ to the present JJA

heating of the atmosphere over the regions adjacent to the East Europe Plateau–Ural Mountains (Figure 15b), increases the local atmospheric thickness (Figure 15c), and thereby contributes to an increased frequency of UB.

The model responses described above suggest that the SICs within the Barents Sea have two separate effects on summertime UB activity. The first effect, weakened polewards temperature gradients causes the mid-latitude (high-latitude) zonal wind to slow (intensify); meanwhile, the decreased mid-latitude STEA enhances the vorticity forcing, which may drive downstream influences. The second thermodynamic effect, reductions in precipitation causes the soil to dry continuously and leads to heating of the atmosphere. Both of these effects likely favour the rise of Z500 over the Ural Mountains and thus the increased frequency of UB events.

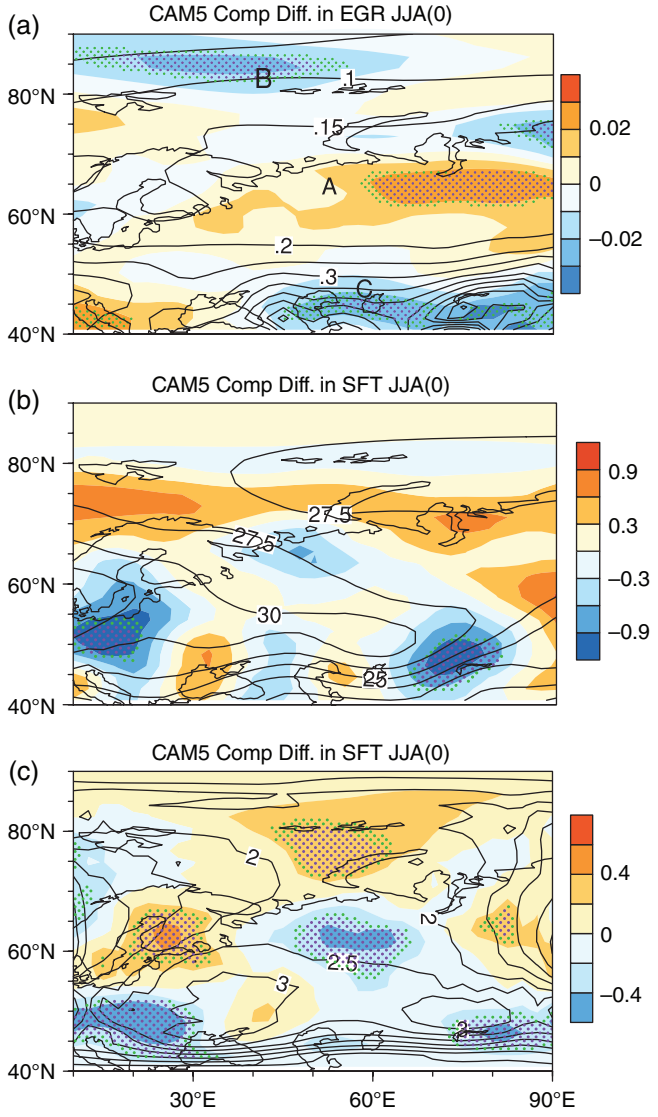

FIGURE 14 The simulated composite differences (shadings) in the JJA (a) 700-hPa EGR, (b) 500-hPa STEA, and (c) 500-hPa SFT between the heavy and light SIC experiments and their climatology in the control run (contours). The letters A (B and C) denote the regions with enhanced (decreased) low-level baroclinicity. Values that significantly exceed the 90 and 95% confidence levels are indicated by green and purple dots, respectively

6 | DISCUSSION AND CONCLUSION

6.1 | Discussion

This study provides evidence of a possible causal link between changes in Arctic sea ice and the large-scale mid-latitude atmospheric circulation in summer, especially the UB frequency. We find that the summertime UB-related wave train differs from its wintertime counterpart in several ways (Wang *et al*., 2010; Cheung and Zhou, 2015). The former appears to be more zonally oriented and constrains the blocking ridge over the Ural Mountains, whereas the latter is more meridionally oriented, and its blocking ridge extends northwards to the Arctic (figure omitted).

In our study, although the model response of geopotential height appears to explain a large fraction of the variability seen in the reanalysis, some discrepancies and uncertainties still exist, which can be difficult to disentangle from internal variability (Deser *et al*., 2010; Screen *et al*., 2013a; 2013b). Previous studies have argued that, in winter, the mid-latitude responses to changes in Arctic sea ice are relatively small when compared to the influence of internal variability (e.g., Screen *et al*., 2013a; 2013b; Sun *et al*., 2016b), whereas those that occur in summer are reasonably large (Petrie *et al*., 2015). Here, we investigate the role of internal variability in the summertime UB responses to anomalous Arctic SIC in both the reanalysis output and the simulation results by calculating their standard deviations (figure omitted). These two patterns both show zonal belt-like structures with large values over the polar and subpolar jet stream regions and small values at lower latitudes. On the one hand, the internal variability resembles the spatial pattern and amplitude between the observations and simulations over vast regions of the mid-latitudes, although the model response to the east of Ural Mountains seems relatively small. On the other hand, the amplitudes of the circulation response over the Ural Mountains in both the observations and simulations are mostly equal to their standard deviations. These analyses imply that the uncertainties in the reanalysis and the simulations may be partly due to internal variability; thus, the effects of the internal variability of the atmosphere must not be neglected when we explore the possible impacts of Arctic sea ice on mid-latitude circulation.

In addition, as noted by Mori *et al*. (2014), whether a robust response of atmospheric circulation to Arctic sea ice could be identified was strongly controlled by the ensemble size. Here, we explore the dependence of the simulated response of the summer UBI to Arctic sea ice on the number of ensemble members. We calculate the probability distribution functions (PDFs) of the UBI in the varying ensembles sizes drawn from the heavy and light SIC experiments (figure omitted). The PDFs of the UBI responses demonstrate that greater numbers of UB events occur in the heavy SIC experiment, and the PDFs narrow as the ensemble size increases gradually from 10 to 50 members. This result indicates that larger ensembles help to reduce the uncertainties arising from the internal variability of the atmosphere.

Moreover, the model-simulated UBI response to Arctic sea ice may also be hampered by several other factors. (a) As indicated by Davini *et al*. (2014), atmospheric blocking is unfortunately one of the phenomena that many climate models have difficulty in simulating, owing to the chaotic nature of atmospheric circulation and the inaccurate representation of atmospheric processes. Hence, many climate models underestimate blocking in Europe (D'Andrea *et al*., 1998; Scaife *et al*., 2010). The model biases may arise from the deficiencies of CAM5.0 in simulating storm tracks (Gettelman *et al*., 2012; Kay *et al*., 2012; Cheung and Zhou,

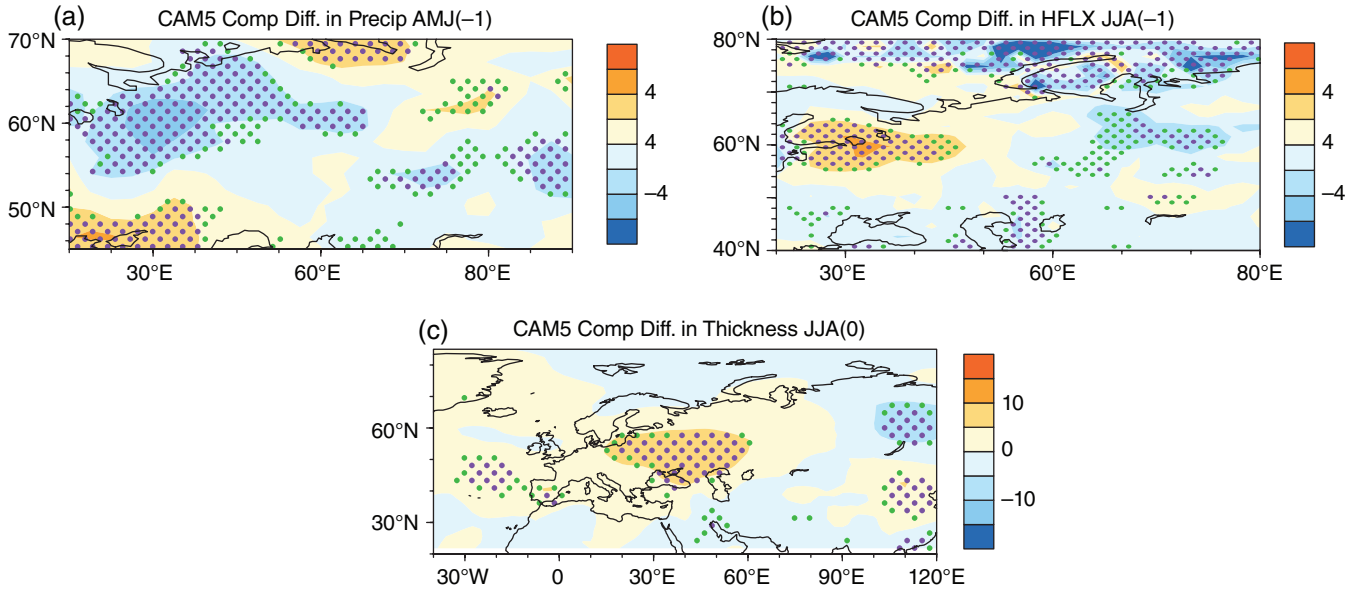

FIGURE 15 The simulated composite differences in (a) the MAM surface heat flux, (b) the April–June Eurasian precipitation, and (c) the low-middle tropospheric thickness (Z500–Z1000) between the heavy and light SIC experiments. Values that significantly exceed the 90 and 95% confidence levels are indicated by green and purple dots, respectively

2015). (b) North Atlantic SSTs and the North Atlantic Oscillation should also be considered as factors that may influence the inter-annual variability of summer UB (e.g., Li and Ji, 2001; Li, 2004; Wu *et al*., 2009b; Zuo *et al*., 2013; Luo *et al*., 2016a). Therefore, achieving a comprehensive understanding of variations in UB frequency in our further studies will require the consideration of multiple external forcings and the internal variability of the atmosphere.

6.2 | Conclusion

The analyses of observations and the numerical simulations using the CAM5.0 model presented in this study support the importance of two mechanisms, dynamic and thermodynamic processes, by which spring–summer Arctic sea ice conditions may influence the inter-annual variations in UB frequency in summer. We find that heavy (light) SICs within the Barents Sea display a statistically significant correlation with increased (decreased) UB frequency in summer, due to a mid-latitude wave train extending over Eurasia. Related to high UB frequency, the presence of exaggerated SICs tends to increase the low-level MTG towards the south which increases zonal winds over the high-latitude regions, and decreases it towards regions surrounding the Ural Mountains which produces slower zonal winds over the mid-latitude regions. Hassanzadeh *et al*. (2014) also agreed that a smaller temperature difference from mid-latitudes to the poles over Eurasia favored the slowing down of mid-latitude zonal winds. The north–south meandering of the jet stream results in the decreased progression of weather systems, which increased the likelihood of UB events. Moreover, the heavy SICs enhances the lower-tropospheric baroclinicity represented by EGR in high-latitude regions and weakens it in mid-latitude regions, facilitating a reduction in STEA that extends from eastern Europe to the Ural Mountains. A related, intense transient eddy-vorticity forcing emerges over the East Europe Plateau, which may increase the probability for more frequent summertime UB events in the downstream regions (Luo *et al*., 2016b; 2017). Based on these analyses, we may conclude that heavy Arctic SICs over the Barents Sea have decelerated the U500 and weakened the STEA over Eurasian mid-latitude regions, which led to the stagnation of UB. It should be noted that heavy SIC-forced U500 and STEA anomalies at high-latitudes tend to shift southeastwards relative to those associated with the frequent UB events. This is because Arctic SIC-induced heat flux anomalies are spatially restricted over southern Barents Sea, which inhibits the northwards expansion of increased U500. Therefore, a comprehensive understanding of UB-related circulation anomalies at high latitudes is necessary to consider the combined impacts of SIC and SM.

From a thermodynamic way, the increase in SICs within the Barents Sea leads to reductions in precipitation over the East Europe Plateau in spring. The possible linkage is hypothesized to be caused by anomalously heavy SIC-driven circulation anomalies and insufficient water vapour released from the frozen ocean, as suggested by Liu *et al*. (2012), which presents such a relationship during autumn. The associated physical mechanisms responsible for this statistical linkage should also be extensively explored in future studies. The deficiency of precipitation subsequently produces dry soil conditions in the following summer and increases the transfer of additional energy from the soil into the mid-latitude atmosphere, leading to amplified atmospheric thickness and to the development of upper-air anticyclonic circulation over the Ural Mountains (Ferranti and Viterbo, 2006;

Zampieri *et al*., 2009). Our results elucidate the thermodynamic role of SM anomalies that are forced by heavy SICs in frequently occurring summer UB events. On the other hand, light SIC conditions would exert the opposite dynamic and thermodynamic effects on the variations in the summertime UB frequency.

As stated above, from a physical point of view, the dynamic and thermodynamic effects of Arctic SICs are statistically and dynamically dependent. To assess the combined effects of the Arctic SICs and Eurasian SMs on the mid-latitude circulation, composite analyses are subsequently applied to corresponding time series. Heavy SICs in MAM and dry soil conditions in JJA tend to drive a significant anticyclonic anomaly over the Ural Mountains, whereas light SICs and wet soil conditions in JJA lead to a cyclonic anomaly. The combined effects of the Arctic SICs and Eurasian SMs reinforce their influence on the presence of a blocking ridge over the Ural Mountains in summer. These statistical analyses provide preliminary evidence for the combined effects of Arctic SICs and soil SMs, and a systematic research plan for the corresponding mechanism should be carried out in future studies. Such efforts will help improve our understanding of the combined impact of multiple external forcings on the summertime climate in Eurasian mid- to high-latitude regions.

ACKNOWLEDGEMENTS

We thank the two reviewers for their helpful comments. This research is supported by the National Basic Research Program of China (Grant No. 2013CB430203), the National Natural Science Foundation of China (Grants Nos. 41790472, 41730959, 41661144017, 41505053), and the China Special Fund for Meteorological Research in the Public Interest (Grant No. GYHY201406018).

ORCID

Ruonan Zhang http://orcid.org/0000-0003-1624-1864
Chenghu Sun http://orcid.org/0000-0002-9462-2390

REFERENCES

Alexander, M.A., Bhatt, U.S., Walsh, J.E., Timlin, M.S., Miller, J.S. and Scott, J. D. (2004) The atmospheric response to realistic Arctic sea ice anomalies in an AGCM during winter. *Journal of Climate*, 17, 890–905.

Bader, J., Mesquita, M.D.S., Hodges, K.I., Keenlyside, N., Osterhus, S. and Miles, M. (2011) A review on Northern Hemisphere sea-ice, storminess and the North Atlantic Oscillation: observations and projected changes. *Atmospheric Research*, 101, 809–834.

Balsamo, G., Viterbo, P., Beljaars, A., Hurk, B.V.D., Hirschi, M., Betts, A.K. and Scipal, K. (2009) A revised hydrology for the ECMWF model. Verification from field site to terrestrial water storage and impact in the integrated forecast system. *Journal of Hydrometeorology*, 10, 623–643.

Barriopedro, D. and Garcia-Herrera, R. (2006) A climatology of Northern Hemisphere blocking. *Journal of Climate*, 19, 1042–1063.

Butler, A.H., Thompson, D.W.J. and Heikes, R. (2010) The steady-state atmospheric circulation response to climate change-like thermal forcings in a simple general circulation model. *Journal of Climate*, 23, 3474–3496.

Cheung, H.H.N. and Zhou, W. (2015) Implications of Ural blocking for East Asian winter climate in CMIP5 GCMs. Part I: biases in the historical scenario. *Journal of Climate*, 28, 2203–2216.

Cohen, J., Jones, J., Furtado, J.C. and Tziperman, E. (2013) Warm Arctic, cold continents: a common pattern related to Arctic sea ice melt, snow advance, and extreme winter weather. *Oceanography.*, 26, 150–160.

D'Andrea, F., Tibaldi, S., Blackburn, M., Boer, G., Déqué, M., Dix, M., Dugas, B., Ferranti, L., Iwasaki, T., Kitoh, A., Pope, V., Randall, D., Roeckner, E., Strauss, D., Stern, W., Van den Dool, H. and Williamson, D.L. (1998) Northern Hemisphere atmospheric blocking as simulated by 15 atmospheric general circulation models in the period 1979–1988. *Climate Dynamics*, 14, 385–407.

Davini, P., Cagnazzo, C., Fogli, P.G., Manzini, E., Gualdi, S. and Navarra, A. (2014) European blocking and Atlantic jet stream variability in the NCEP/NCAR reanalysis and the CMCC-CMS climate model. *Climate Dynamics*, 43, 71–85.

Davis, R. (1976) Predictability of sea surface temperature and sea level pressure anomalies over the North Pacific Ocean. *Journal of Physical Oceanography*, 6, 249–266. https://doi.org/10.1175/1520-0485(1976)006,0249:POSSTA.2.0.CO;2.

Deser, C., Tomas, R. and Peng, S. (2007) The transient atmospheric circulation response to North Atlantic SST and sea ice anomalies. *Journal of Climate*, 20, 4751–4767. https://doi.org/10.1175/jcli4278.1.

Deser, C., Tomas, R., Alexander, M. and Lawrence, D. (2010) The seasonal atmospheric response to projected Arctic sea ice loss in the late twenty first century. *Journal of Climate*, 23, 333–351.

Dethloff, K., et al. (2006) A dynamical link between the Arctic and the global climate system. *Geophysical Research Letters*, 33, L03703. https://doi.org/10.1029/2005GL025245.

Duchon, C. (1979) Lanczos filtering in one and two dimensions. *Journal of Applied Meteorology*, 18, 1016–1022.

Fang, J. and Yang, X.Q. (2016) Structure and dynamics of decadal anomalies in the wintertime midlatitude North Pacific Ocean–atmosphere system. *Climate Dynamics*, 47, 1989–2007. https://doi.org/10.1007/s00382-015-2946-x.

Ferranti, L. and Viterbo, P. (2006) The European summer of 2003: sensitivity to soil water initial conditions. *Journal of Climate*, 19, 3659–3680.

Fischer, E.M., Seneviratne, S.I., Vidale, P.L., Luthi, D. and Schar, C. (2007) Soil moisture-atmosphere interactions during the 2003 European summer heat wave. *Journal of Climate*, 20(20), 5081–5099.

Francis, J.A. and Vavrus, S.J. (2012) Evidence linking Arctic amplification to extreme weather in midlatitudes. *Geophysical Research Letters*, 39, L06801. https://doi.org/10.1029/2012GL051000.

Gettelman, A., Kay, J.E. and Shell, K.M. (2012) The evolution of climate sensitivity and climate feedbacks in the community atmosphere model. *Journal of Climate*, 25, 1453–1469.

Hassanzadeh, P. and Kuang, Z. (2015) Blocking variability: Arctic amplification versus Arctic Oscillation. *Geophysical Research Letters*, 42(20), 8586–8595.

Hassanzadeh, P., Kuang, Z. and Farrell, B.F. (2014) Responses of midlatitude blocks and wave amplitude to changes in the meridional temperature gradient in an idealized dry GCM. *Geophysical Research Letters*, 41, 5223–5232. https://doi.org/10.1002/2014GL060764.

Honda, M., Inoue, J. and Yamane, S. (2009) Influence of low Arctic sea ice minima on anomalously cold Eurasian winters. *Geophysical Research Letters*, 36, L08707.

Hoskins, B.J. and Valdes, P.J. (1990) On the existence of storm-tracks. *Journal of Atmospheric Sciences*, 47, 1854–1864.

Hoskins, B.J., James, I.N. and White, G.H. (1983) The shape, propagation and mean-flow interaction of large-scale weather systems. *Journal of the Atmospheric Sciences*, 40, 1595–1612.

Jaiser, R., Dethloff, K., Handorf, D., Rinke, A. and Cohen, J. (2012) Impact of sea-ice cover changes on the Northern Hemisphere atmospheric winter circulation. *Tellus A*, 64, 11595. https://doi.org/10.3402/tellusa.v64i0.11595.

Kalnay, E., Kanamitsu, M., Kistler, R., Collins, W.G., Deaven, D., Gandin, L.S., Iredell, M., Saha, S., White, G., Woollen, J., Zhu, Y., Chelliah, M., Ebisuzaki, W., Higgins, W., Janowiak, J.E., Mo, K.C., Ropelewski, C., Wang, J. and Leetmaa, A. (1996) The NCEP/NCAR 40-year reanalysis project. *Bulletin of the American Meteorological Society*, 77, 437–471.

Kay, J.E., Hillman, B.R., Klein, S.A., Zhang, Y., Medeiros, B., Pincus, R., Gettelman, A., Eaton, B., Boyle, J., Marchand, R. and Ackerman, T.P. (2012) Exposing global cloud biases in the Community Atmosphere Model

(CAM) using satellite observations and their corresponding instrument simulators. *Journal of Climate*, 25, 5190–5207.

Kug, J.S. and Jin, F.F. (2009) Left-hand rule for synoptic eddy feedback on low-frequency flow. *Geophysical Research Letters*, 36, L05709. https://doi.org/10.1029/2008GL036435.

Lau, N.C. and Holopainen, E.O. (1984) Transient eddy forcing of the time-mean flow as identified by geopotential tendencies. *Journal of the Atmospheric Sciences*, 41, 313–328.

Li, S.L. (2004) Influence of the northwest Atlantic SST anomaly on the circulation over the Ural Mountains. *Journal of the Meteorological Society of Japan*, 82, 971–988.

Li, S.L. and Ji, L.R. (2001) Background circulation characteristics of the persistent anomalies of the summertime circulation over the Ural Mountains. *Acta Meteorologica Sinica*, 59, 280–293 (in Chinese).

Li, F. and Wang, H.J. (2012) Autumn sea ice cover, winter Northern Hemisphere annular mode and winter precipitation in Eurasia. *Journal of Climate*, 26, 3968–3981.

Li, F. and Wang, H.J. (2014) Autumn Eurasian snow depth, autumn Arctic sea ice cover and East Asian winter monsoon. *International Journal of Climatology*, 34, 3616–3625.

Lindzen, R.S. and Farrell, B. (1980) A simple approximate result for the maximum growth rate of baroclinic instabilities. *Journal of the Atmospheric Sciences*, 37, 1648–1654.

Liu, Z.Y. and Alexander, M. (2007) Atmospheric bridge, oceanic tunnel, and global climate teleconnections. *Reviews of Geophysics*, 45, RG2005.

Liu, X. and Yanai, M. (2002) Influence of Eurasian spring snow cover on Asian summer rainfall. *International Journal of Climatology*, 22, 1075–1089.

Liu, J.P., Curry, J.A., Wang, H.J., Song, M.R. and Horton, R.M. (2012) Impact of declining Arctic sea ice on winter snowfall. *Proceedings of the National Academy of Sciences of the United States of America*, 109, 4074–4079.

Liu, Y.Y., Wang, L., Zhou, W. and Chen, W. (2014) Three Eurasian teleconnection patterns: spatial structures, temporal variability, and associated winter climate anomalies. *Climate Dynamics*, 42, 2817–2839.

Luo, D., Xiao, Y., Yao, Y., Dai, A., Simmonds, I. and Franzke, C.L.E. (2016a) Impact of Ural blocking on winter warm arctic-cold Eurasian anomalies. Part I: blocking-induced amplification. *Journal of Climate*, 29, 3925–3947.

Luo, D., Xiao, Y., Yao, Y., Dai, A., Franzke, C.L.E. and Simmonds, I. (2016b) Impact of Ural blocking on winter warm arctic-cold Eurasian anomalies. Part II: the link to the North Atlantic oscillation. *Journal of Climate*, 29, 3949–3971.

Luo, D., Yao, Y., Dai, A., Simmonds, I. and Zhong, L. (2017) Increased quasi stationarity and persistence of winter Ural blocking and Eurasian extreme cold events in response to Arctic warming. Part II: a theoretical explanation. *Journal of Climate*, 30(10), 3569–3587.

Miralles, D.G., Teuling, A.J., Heerwaarden, C.C. and Arellano, J.V. (2014) Mega-heatwave temperatures due to combined soil desiccation and atmospheric heat accumulation. *Nature Geoscience*, 7, 345–349.

Mori, M., Watanabe, M., Shiogama, H., Inoue, J. and Kimoto, M. (2014) Robust Arctic sea-ice influence on the frequent Eurasian cold winters in past decades. *Nature Geoscience*, 7, 869–873.

Murray, R.J. and Simmonds, I. (1995) Responses of climate and cyclones to reductions in Arctic sea ice. *Journal of Geophysical Research*, 100, 4791–4806.

Nakamura, H. and Wallace, J.M. (1993) Synoptic behavior of baroclinic eddies during the blocking onset. *Monthly Weather Review*, 121, 1892–1903.

Newson, R.L. (1973) Response of general circulation model of the atmosphere to removal of the 13 Arctic ice cap. *Nature*, 241, 39–40.

Palmén, E. and Newton, C.W. (1969) *Atmospheric Circulation Systems: Their Structure and Physical Interpretation*. New York, NY: Academic Press.

Peings, Y. and Magnusdottir, G. (2014) Response of the wintertime Northern Hemisphere atmospheric circulation to current and projected Arctic sea ice decline: a numerical study with CAM5. *Journal of Climate*, 27, 244–264.

Petoukhov, V. and Semenov, V. (2010) A link between reduced Barents–Kara sea-ice and cold winter extremes over northern continents. *Journal of Geophysical Research*, 115, D21111. https://doi.org/10.1029/2009JD013568.

Petrie, R.E., Shaffrey, L.C. and Sutton, R.T. (2015) Atmospheric response in summer linked to recent Arctic sea ice loss. *Quarterly Journal of the Royal Meteorological Society*, 141, 2070–2076.

Rayner, N.A., Parker, D.E., Horton, E.B., Folland, C.K., Alexander, L.V., Rowell, D.P., Kent, E.C. and Kaplan, A. (2003) Global analyses of sea surface temperature, sea ice, and night marine air temperature since the late nineteenth century. *Journal of Geophysical Research*, 108, 4407.

Ren, H.L., Jin, F.F., Kug, J.S., Zhao, J.X. and Park, J. (2009) A kinematic mechanism for positive feedback between synoptic eddies and NAO. *Geophysical Research Letters*, 36, L11709. https://doi.org/10.1029/2009GL037294.

Sato, K., Inoue, J. and Watanabe, M. (2014) Influence of the Gulf Stream on the Barents Sea ice retreat and Eurasian coldness during early winter. *Environmental Research Letters*, 9, 084009.

Scaife, A.A., Woollings, T., Knight, J., Martin, G. and Hinton, T. (2010) Atmospheric blocking and mean biases in climate models. *Journal of Climate*, 23, 6143–6152.

Screen, J.A., Simmonds, I., Deser, C. and Tomas, R. (2013a) The atmospheric response to three decades of observed arctic sea ice loss. *Journal of Climate*, 26, 1230–1248.

Screen, J.A., Deser, C., Simmonds, I. and Tomas, R. (2013b) Atmospheric impacts of Arctic sea-ice loss, 1979–2009: separating forced change from atmospheric internal variability. *Climate Dynamics*, 43, 333–344.

Shutts, B.G.J. (1983) The propagation of eddies in diffluent jet streams: eddy vorticity forcing of "blocking" flow fields. *Quarterly Journal of the Royal Meteorological Society*, 109, 737–761.

Simmonds, I. (2015) Comparing and contrasting the behaviour of Arctic and Antarctic sea ice over the 35-year period 1979–2013. *Annals of Glaciology*, 56, 18–28.

Simmonds, I. and Govekar, P.D. (2014) What are the physical links between arctic sea ice loss and Eurasian winter climate? *Environmental Research Letters*, 9, 101003. https://doi.org/10.1088/1748-9326/9/10/101003.

Sun, C.H., Yang, S., Li, W.J., Zhang, R.N. and Wu, R.G. (2016a) Interannual variations of the dominant modes of East Asian winter monsoon and possible links to Arctic sea ice. *Climate Dynamics*, 47, 481–496.

Sun, L.T., Perlwitz, J. and Hoerling, M. (2016b) What caused the recent "warm arctic, cold continents" trend pattern in winter temperatures? *Geophysical Research Letters*, 43, 5345–5352.

Tang, Q.H., Zhang, X.J., Yang, X.H. and Jennifer, A.F. (2013) Cold winter extremes in northern continents linked to Arctic sea ice loss. *Environmental Research Letts*, 8, 014036.

Tang, Q.H., Zhang, X.J. and Francis, J.A. (2014) Extreme summer weather in northern mid-latitudes linked to a vanishing cryosphere. *Nature Climate Chanage*, 4, 45–50.

Tao, S.Y. (1980) *Heavy Rainfalls in China*. Beijing: Science Press, 225 pp. (in Chinese).

Tibaldi, S. and Molteni, F. (1990) On the operational predictability of blocking. *Tellus A*, 42, 343–365.

Wang, L. and Chen, W. (2014) The East Asian winter monsoon: re-amplification in the mid-2000s. *Chinese Science Bulletin*, 59, 430–436.

Wang, L. and Gu, W. (2016) The eastern China flood of June 2015 and its causes. *Science Bulletin*, 61, 178–184.

Wang, L., Chen, W., Zhou, W., Chan, J., Barriopedro, D. and Huang, R.H. (2010) Effect of the climate shift around mid 1970s on the relationship between wintertime ural blocking circulation and East Asian climate. *International Journal of Climatology*, 30, 153–158.

Williams, R.G., Wilson, C. and Hughes, C.W. (2007) Ocean and atmosphere storm tracks: the role of eddy vorticity forcing. *Journal of Physical Oceanography*, 37, 2267–2289.

Woollings, T., Harvey, B. and Masato, G. (2014) Arctic warming, atmospheric blocking and cold European winters in CMIP5 models. *Environmental Research Letters*, 9, 014002.

Wu, B.Y., Huang, R.H. and Gao, D. (1999) Impact of variations of winter sea-ice extents in the Kara/Barents seas on winter monsoon over East Asia. *Acta Meteorologica Sinica*, 13, 141–153.

Wu, B.Y., Zhang, R.H. and Wang, B. (2009a) On the association between spring Arctic sea ice concentration and Chinese summer rainfall: a further study. *Advances in Atmospheric Sciences*, 26, 666–678.

Wu, Z.W., Wang, B., Li, J.P. and Jin, F.F. (2009b) An empirical seasonal prediction model of the East Asian summer monsoon using ENSO and NAO. *Journal of Geophysical Research*, 114, D18120. https://doi.org/10.1029/2009jd011733.

Wu, B.Y., Su, J.Z. and Zhang, R.H. (2011) Effects of autumn-winter arctic sea ice on winter Siberian high. *Chinese Science Bulletin*, 56, 3220–3228.

Wu, B.Y., Zhang, R.H., D'Arrigo, R. and Su, J.Z. (2013) On the relationship between winter sea ice and summer atmospheric circulation over Eurasia. *Journal of Climate*, 26, 5523–5536.

Xie, P., Yatagai, A., Chen, M., Hayasaka, T., Fukushima, Y., Liu, C. and Yang, S. (2007) A gauge-based analysis of daily precipitation over East Asia. *Journal of Hydrometeorology*, 8, 607–626.

Yao, Y., Luo, D., Dai, A. and Simmonds, I. (2017) Increased quasi stationarity and persistence of winter Ural blocking and Eurasian extreme cold events in response to Arctic warming. Part I: insights from observational analyses. *Journal of Climate*, 30(10), 3549–3568.

Zampieri, M., D'Andrea, F., Vautard, R., Ciais, P., Noblet, D. and Yiou, P. (2009) Hot European summers and the role of soil moisture in the propagation of Mediterranean drought. *Journal of Climate*, 22(18), 4747–4758.

Zhang, Q.Y. and Tao, S.Y. (1998) Influence of Asian mid-high latitude circulation on East Asian summer rainfall. *Acta Meteorologica Sinica*, 56, 199–211 (in Chinese).

Zhang, Q.Y. and Tao, S.Y. (2001) A study of excessively heavy rainfall in the Songhuajiang–Nenjiang River valley in 1998. *Chinese Journal of Atmospheric Sciences*, 4, 567–576 (in Chinese).

Zuo, J.Q., Li, W.J., Sun, C.H., Xu, L. and Ren, H.L. (2013) The impact of North Atlantic sea surface temperature tripole on the East Asian summer monsoon. *Advances in Atmospheric Sciences*, 30, 1173–1186.

How to cite this article: Zhang R, Sun C, Zhang R, Jia L, Li W. The impact of Arctic sea ice on the interannual variations of summer Ural blocking. *Int J Climatol*. 2018;38:4632–4650. https://doi.org/10.1002/joc.5731